LA-3619

C.3

LOS ALAMOS SCIENTIFIC LABORATORY
of the
University of California
LOS ALAMOS • NEW MEXICO

Effective Two-Group Gamma-Ray Spectra for Thermal Neutron Capture and Prompt Fission

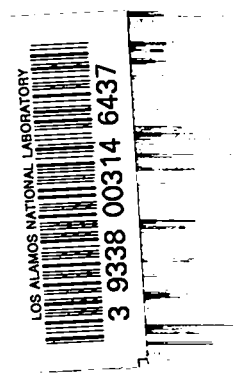

UNITED STATES
ATOMIC ENERGY COMMISSION
CONTRACT W-7405-ENG. 36

This report expresses the opinions of the author or authors and does not necessarily reflect the opinions or views of the Los Alamos Scientific Laboratory.

Printed in the United States of America. Available from Clearinghouse for Federal Scientific and Technical Information National Bureau of Standards, U. S. Department of Commerce Springfield, Virginia 22151

Price: Printed Copy $3.00; Microfiche $0.65

LA-3619
UC-80, REACTOR
TECHNOLOGY
TID-4500

LOS ALAMOS SCIENTIFIC LABORATORY
of the
University of California
LOS ALAMOS • NEW MEXICO

Report written: October 1966
Report distributed: February 10, 1967

Effective Two-Group Gamma-Ray Spectra for Thermal Neutron Capture and Prompt Fission

by

Donald J. Dudziak

ABSTRACT

Effective two-group gamma-ray spectra were determined for thermal neutron capture in sodium, nickel, type 304 stainless steel, and tantalum, as well as for ^{235}U prompt fission gamma rays. The absorbed dose due to uncollided and built-up fluxes in several materials was calculated for varying thicknesses of several intervening shielding materials. A seven-group compilation of capture gamma rays and an analytical fit to the prompt fission gamma-ray spectrum were used as the basis for this study. The resulting function for each combination of shielding and absorbing material was reduced to two exponential functions for areal density ranges with upper limits as great as 560 g/cm^2. These effective spectra reproduce, to within an average absolute deviation of less than 7.4 percent, the absorbed doses (uncollided and built-up) calculated by the detailed spectra, within the ranges of areal density considered.

ACKNOWLEDGEMENTS

The author is grateful to N. K. Madsen, who did the preliminary FORTRAN IV coding of the calculations and plotting, and to M. E. Battat for his assistance and helpful consultation on this entire work, especially for the determination of total and energy absorption mass attenuation coefficients for tantalum.

I. INTRODUCTION AND SUMMARY

Basic data on the spectral distribution of gamma rays emitted in neutron radiative capture reactions are usually too detailed to be directly useful for shielding calculations. It thus becomes necessary to collate the data into some convenient energy group structure. Many authors[1-3] have condensed the data into energy group structures of manageable size (five to ten groups) for routine shielding calculations, without compromising the reliability of information extracted from the calculations (e.g., absorbed dose in various materials, including tissue). Mittelman and Liedtke[1] used a five-group structure and a maximum photon energy listing, while Deloume[2] used a ten-group structure. More recently, Troubetzkoy and Goldstein[3] have compiled a seven-group table for most elements of interest; included in the compilation are decay gamma rays from product nuclei with half-lives of the order of hours or less. This seven-group tabulation was used for most of the detailed-spectrum calculations reported herein. It also presents tabulations of line spectra and graphs of differential spectra, which update the work of Bartholomew and Higgs.[4]

Shure and Strobel[5] further reduced the compilations of Deloume[2] and Lanning (unpublished) to effective two-group capture spectra (a three-group spectrum in the case of prompt fission gamma rays) for several common materials of interest to the naval reactors program: iron, zirconium, hafnium, ^{238}U, and stainless steel (SS). In unpublished work quoted by Guilinger, et al.,[6] the author and Schmucker performed the same reduction for Inconel-X (73 w/o nickel, 17 w/o chromium, 10 w/o iron).

This report presents an extension of these results to materials of interest for fast reactors: sodium, nickel, type 304 stainless steel (new spectrum), and tantalum. In addition, a two-group effective ^{235}U prompt fission gamma-ray spectrum has been calculated. A FORTRAN IV program has been written to perform all the calculations, plotting, and curve fitting, so an extension to other spectra is facilitated.

All these effective spectra differ from the many-group spectra in that they were not arrived at by an energy grouping process, but rather by an analytical fitting of typical absorbed dose calculations for various attenuating and absorbing materials. The resulting spectra are then "effective" only in the context of shielding calculations using these materials.

The procedure is, briefly, to calculate for the many-group source spectra the absorbed dose in various materials following varying thicknesses of attenuating material. Both absorbing and attenuating materials cover a wide range of atomic numbers. For each absorbing material (a parameter), the absorbed dose from a unit plane monodirectional source with the many-group spectrum is determined as a function of areal density (g/cm^2) of each attenuating material. Each of the resulting functions is then fitted asymptotically by a single exponential, and a corresponding effective energy is determined from the exponent. From the results of many such asymptotic fits, a single energy representative of the attenuation coefficient is chosen, and an attenuation curve for this energy is normalized in the asymptotic region of each function. Residuals are then determined by subtraction of the normalized exponential attenuation curves from the original attenuation curves. Successive representative effective energies are chosen by repeating the fitting process on the residuals. From the intercepts of the exponential curve for each representative energy, effective gamma-ray energy yields are determined. A summary of these yields is presented in Table I.

Most of the capture gamma-ray data accumulated to date have been for thermal neutron capture. These data are normally regarded as being sufficiently accurate for shielding calculations, when used for radiative capture reactions at all energies for which the cross section is significant (up to roughly 100 keV). In some cases, as in the shielding of some fast reactors, these reactions may occur predominantly in the 1 to 100 keV range, opening this assumption to some question. However, for most shield materials of concern, the binding energy of the incident neutron is of the order of 8 MeV, so the total photon energy emitted (essentially equal to the neutron binding energy plus the neutron kinetic energy) does not differ much from the binding energy. This is not to say, however, that the spectrum does not differ significantly. This matter is discussed by Troubetzkoy and Goldstein.[3,7] For lack of better data, the thermal neutron capture spectra are used in practice and have thus far presented no unacceptable discrepancies. Similarly, the prompt gamma-ray spectrum from thermal neutron-induced fission is used for higher energy fission.

Test calculations of uncollided absorbed doses using the two-group effective spectra show remarkable agreement with comparable many-group calculations over a large range of areal densities. Specific cases are included in the data given in Tables II through VI. These tables list the maximum areal densities over which comparisons were made with many-group uncollided absorbed doses, the total number of points (i.e., shield thicknesses) at which comparisons were made, the average absolute deviation for the points at which the comparisons were made, the maximum deviation in this range, and the areal density at which the maximum deviation occurs. All these results are for uncollided absorbed dose. Similar results have been obtained with the built-up absorbed dose, as shown in Tables VII through XI. These results were based upon Taylor's buildup parameters, as given by Guilinger, et al.[6] Figure 1 shows a typical attenuation plot (asterisks) in iron, the two effective spectrum curves, and the sum of the two effective spectrum curves. All these curves are for the uncollided absorbed dose in carbon.

Comparisons were also made between the present effective spectra and Shure and Strobel's effective spectra for type 304 stainless steel and prompt fission. The results of uncollided and built-up absorbed dose calculations using the different sets of effective spectra agree reasonably well and indicate that the present effective spectra may be applicable at deeper penetrations than the spectra of Shure and Strobel.

Considering the uncertainties in the raw data from which the many-group compilations are derived,[3] the effective two-group spectra should prove adequate for practical shielding calculations. They should be particularly useful where calculations are performed without the aid of a computer code.

II. CALCULATIONAL PROCEDURE

A. Determination of Many-Group Spectra

The many-group (five or six) capture gamma-ray yields (MeV/capture) were determined by use of the energy groupings of Troubetzkoy and Goldstein. The only modification in these energy groupings was that the >9 MeV group was combined with that for 7-9 MeV, resulting in six groups: 0-1, 1-2, 2-3, 3-5, 5-7, and 7-9+ MeV. Troubetzkoy and Goldstein give the number of photons in each energy group per 100 captures. In cases where the product nucleus has a half-life of the order of hours or less, the decay gamma rays were included in the tabulation. In order to determine the total energy emitted in each group, the discrete gamma-ray energies and intensities were used, wherever available, to find a weighted average energy in each group. Photons in a group which were not accounted for in the line spectra tabulation were then assigned the median energy of the group in the weighting process. In other words, the weighted average energy in the jth group, $\tilde{E}_j$, is given by

$$\tilde{E}_j = \left\{ \sum_{\nu} E_{j\nu} f_{j\nu} + \left[f_j - \sum_{\nu} f_{j\nu} \right] E_j \right\} f_j^{-1} \quad \text{(MeV)}, \qquad (1)$$

where

$E_{j\nu} \triangleq$ the energy, in MeV, of the νth line spectrum in group j,

$E_j \triangleq$ the median energy, in MeV, of group j,

$f_{j\nu} \triangleq$ the photon yield, in photons/capture, at the energy of the νth line spectrum in group j, and

$f_j \triangleq$ the total photon yield, in photons/capture, of group j.

The gamma-ray energy yield in group j, $Y(E_j)$, is then given by

$$Y(E_j) = f_j \tilde{E}_j \qquad \text{(MeV/capture)}, \tag{2}$$

where E_j is the upper limit of energy group j. Values for $E_{j\nu}$ and $f_{j\nu}$ were determined from Table 2 of Troubetzkoy and Goldstein, and values for f_j were determined from their Table 1. In some cases, insufficient line spectra were given (none for tantalum) to enable the use of this weighting scheme, so $\tilde{E}_j$ was assigned the group median energy, or a value was estimated from Troubetzkoy and Goldstein's curves of the differential capture spectra. The groups are numbered 1 through 6, beginning at the lowest energy (0-1 MeV is group 1, 1-2 MeV is group 2, etc.).

For tantalum capture gamma rays, $f_6 = 0$, and the differential spectrum curve shows no photon yield above 6 MeV. Thus, the fifth group for tantalum was changed to 5-6 MeV.

To determine the six-group spectrum of type 304 stainless steel, the individual elemental components were weighted by their 2200 m/sec macroscopic capture cross sections as follows:

$$Y(E_j) = \frac{\sum_i (w/o)_i \frac{\sigma_i}{A_i} Y_i(E_j)}{\sum (w/o)_i \frac{\sigma_i}{A_i}} \qquad \text{(MeV/capture)}. \tag{3}$$

Here

$(w/o)_i \triangleq$ the weight percent of the ith element in type 304 stainless steel,

$\sigma_i \triangleq$ the 2200 m/sec microscopic capture cross section, in barns, of the ith material in stainless steel, and

$A_i \triangleq$ the atomic weight of the ith material in stainless steel.

Stainless steel was assumed to have the nominal composition for type 304 stainless steel:[8] 71 w/o iron, 19 w/o chromium, and 10 w/o nickel. Trace elements such as magnesium and cobalt have lower weight percents

than the allowable variation in weight percent of the three major constituents; they were, therefore, ignored. Values of σ_i were determined from the compilation of Hughes and Schwartz.[9]

The prompt fission gamma-ray yields for ^{235}U were determined from the analytical fits of the differential prompt fission spectrum data of Maienschein, et al.,[10] as given by Goldstein. The analytical expressions for the differential energy spectrum are

$$I(E) = 26.8\ E \exp(-2.30E) \qquad 0.3 \leq E \leq 1.0 \qquad (\text{fission}^{-1}), \tag{4}$$

$$I(E) = 8.0\ E \exp(-1.10E) \qquad 1.0 \leq E \leq 7 \qquad (\text{fission}^{-1}), \tag{5}$$

where

$I(E) \triangleq$ the differential prompt fission gamma-ray energy spectrum (MeV/fission-MeV).

These data are for gamma rays emitted with $\simeq 5 \times 10^{-8}$ sec after thermal fission of ^{235}U. Kirkbride[11] has shown that there is no observable difference in the prompt gamma spectral shapes for ^{235}U, ^{233}U, and ^{239}Pu fission. The seven-group spectrum for prompt fission was then determined by integration of Eqs. (4) and (5) over the appropriate ranges; e.g.,

$$Y(1\ \text{MeV}) = 26.8 \int_{0.3}^{1.0} E \exp(-2.30E)\, dE \qquad (\text{MeV/fission}). \tag{6}$$

In general,

$$Y(E_j) = 8.0 \int_{E_{j-1}}^{E_j} E \exp(-1.10E)\, dE \qquad (\text{MeV/fission}), \tag{7}$$

for $j > 1$. Here, we assign the energy released within a group to the upper limit of the group, which is E_j. The resulting seven groups were 0.3-1, 1-2, 2-3, 3-4, 4-5, 5-6, and 6-7 MeV.

Both capture and prompt fission gamma-ray yields in any given group were associated with the upper limit of the energy range of that group. Thus, the gamma-ray attenuation and energy absorption coefficients for these groups are characteristic of this upper limit. As was shown in test calculations by Shure and Strobel[5] for the cases they studied, this assumption is usually conservative. In their study, they used the physical properties (attenuation and absorption coefficients) of the median of the group for several test cases. In an indirect comparison with the results using the upper limit of the group, they showed that no significant changes occurred.

Table XII presents the resulting many-group spectra for capture and prompt fission gamma rays, as determined by the procedure described above. Observe that the total energy includes decay gamma rays for product nuclei with half-lives of less than a day. The binding energies are listed for informational purposes from the tabulation of Deloume,[2] who determined a weighted-average value from the following expression:

$$\text{B.E.} = \frac{\sum_i P_i \, \sigma_i \, (\text{B.E.})_i}{\sum_i P_i \, \sigma_i} \qquad \text{(MeV)}, \tag{8}$$

where

$(\text{B.E.})_i \triangleq$ the binding energy, in MeV, of the extra neutron in the $\underline{(i+1)}$th isotope,

$P_i \triangleq$ the percent abundance of the $\underline{i}$th isotope, and

$\sigma_i \triangleq$ the thermal neutron capture cross section, in barns, of the $\underline{i}$th isotope.

No attempt was made to manipulate the many-group spectrum yields to normalize to the binding energies.

B. Reduction to Two-Group Effective Spectra

If the many-group spectrum is known, the absorbed dose can then be determined for a plane monodirectional beam having this spectrum. Consider a semi-infinite slab of material i, with its surface normal to the beam and an infinitesimal absorbing sphere of material k at an areal density of t_i g/cm^2 along a normal to the surface. Assuming infinite linear electron stopping power (-dE/dx) for both absorber and shield, the uncollided absorbed dose rate in material k from a unit (one event/cm^2) monodirectional beam is given by

$$H_u^k(t_i) = \sum_j \chi_a^k(E_j)\ Y(E_j)\ \exp[-\chi^i(E_j)\ t_i] \qquad \text{(MeV/g)}, \qquad (9)$$

where

$\chi_a^k(E_j) \triangleq$ the energy absorption mass attenuation coefficient, in cm^2/g, of material k, and

$\chi^i(E_j) \triangleq$ the total mass attenuation coefficient of material i, in cm^2/g.

With the exception of tantalum, values of χ_a^k and χ^i were determined from calculations by Blizard, et al.,[12] who used Grodstein's data.[13] For tantalum, these values were determined by M. E. Battat of LASL from the data for pair production and photoelectric effect reported by Storm, et al.,[14] and a computed Compton scatter cross section.

For each many-group spectrum, values of $H_u^k(t_i)$ were determined with 20 combinations of attenuating and absorbing materials. There are five of each type of material as follows:

Attenuating Material	Absorbing Material
iron	iron
carbon	carbon
sodium	tantalum
tantalum	concrete
concrete	tissue

The combinations chosen can be seen in the first and third columns of Tables II through XI. Certain combinations were considered to be of marginal practical interest and were, therefore, ignored (e.g., attenuation in tantalum and absorption in tissue). This decision was made to avoid weighting the effective spectrum results by cases of limited concern, because each combination has equal weight in the averaging of effective yields for any given absorbing material. However, once the calculations were coded, it required little extra effort to test the effective spectra on the combinations of limited interest. Such tests give some indication of the validity of these effective spectra for combinations not among those used in the weighting process. Tables XIII and XIV present a summary of these results, for uncollided and built-up absorbed dose, respectively. These results support extending the effective spectra to cases not used in the weighting process. The maximum deviations are generally larger than for the cases used in the weighting process, but are still acceptable.

Consider now any of the five spectra which were reduced. The calculational procedure is as follows: After computing values of $H_u^k(t_i)$ by Eq. (9) for t_i over a range varying from 0 up to 560 g/cm^2 of material i, we fit the resulting values by an exponential function in the asymptotic region. Figure 2 shows a typical asymptotic fit, for the case of a sodium capture spectrum, iron shield, and carbon absorber. The values of $H_u^k(t_i)$ are plotted with an asterisk. Letting the asymptotic exponential be given by $A_i^k \exp(-\alpha_i^k t_i)$, we have 20 sets (A_i^k, α_i^k), corresponding to the 20 combinations of attenuating and absorbing materials. The determination of the asymptotic region was arbitrary and varied depending upon the maximum areal densities considered for each attenuating material. Again, the maximum areal densities are arbitrary parameters, so they were chosen to exceed any shield thickness anticipated for the material in question in a reactor application. An additional restraint on maximum areal densities was a desire to keep reasonable accuracy of the two-group representation in the ranges of most usual interest. The values chosen are listed in Tables II through VI.

All exponential fitting was performed by a general least-squares subroutine with a weighting option,[15] rather than a linear least-squares fit on transformed data. For the asymptotic exponential, $A_i^k \exp(-\alpha_i^k t_i)$, the weights were the reciprocal of the square of the ordinates, i.e., $w_1^k(t_i) = [H_u^k(t_i)]^{-2}$. This weighting scheme biases the fit toward the asymptotic region. It is equivalent to minimizing, with a weight of $[H_u^k(t_i)]^{-1}$, percent error. Both parameters, A_i^k and α_i^k, were allowed to vary, and an average value of α_i^k was calculated for each material i by the expression

$$\langle \alpha_i^k \rangle_k = \frac{\sum_{k=1}^{N(i)} \alpha_i^k}{N(i)}, \tag{10}$$

where N depends upon i (see Tables II through VI). From these values of $\langle \alpha_i^k \rangle_k$, a representative energy $\bar{E}_1$ was determined for the attenuation in the asymptotic region, giving a consistent set of values, say $\hat{\alpha}_i$, for this energy. The energy $\bar{E}_1$ is the higher energy given in Table I for each spectrum studied. Observe that $\bar{E}_1$ is not in all cases unique for a given attenuating material because the $\chi^i(E)$ have minima, but one energy approximately satisfies all attenuating materials considered. The symbol $\bar{E}_j$ is used to differentiate the effective energies from the many-group energies E_j. With these values of $\hat{\alpha}_i$ held fixed, the least-squares fit was repeated with the A_i^k left as free parameters. The same weights as in the previous fit were used. With all asymptotic slopes in a semi-log plot normalized to a particular energy (the $\hat{\alpha}_i$ are the total mass attenuation coefficients for the effective energy of the asymptotic exponential), the result of this second fitting process is to determine the intercepts $\mathring{A}_i^k$ for a fixed slope $\hat{\alpha}_i$. Referring to Eq. (9), observe that the $\mathring{A}_i^k$ may then be averaged over i to determine an average gamma-ray energy yield at $\bar{E}_1$ MeV, for any fixed k. That is,

$$Y^k(\bar{E}_1) = \frac{\sum_{i=1}^{M(k)} {}^{\circ}A_i^k}{N(k)\,\chi_a^k(\bar{E}_1)}, \tag{11}$$

where M depends upon k (see Tables II through VI). By continuing the averaging process to k, the effective yield at energy $\bar{E}_1$ is found to be

$$\bar{Y}(\bar{E}_1) = \frac{1}{5}\sum_{k=1} Y^k(\bar{E}_1), \tag{12}$$

where we use the symbol $\bar{Y}$ to differentiate the effective yield from the many-group yields. This averaging process gives equal weight to each absorbing material, not to each combination of attenuating and absorbing materials.

Now, let us define parameters

$$A^k(\bar{E}_1) = \chi_a^k(\bar{E}_1)\ \bar{Y}(\bar{E}_1), \tag{13}$$

which in conjunction with the $\hat{\alpha}_i$ completely determine a consistent set of asymptotic attenuation curves $A^k \exp(-\hat{\alpha}_i\ t_i)$, for each of the 20 combinations (i,k). These curves correspond to the higher-energy yields and energies in Table I. Subtracting these asymptotic attenuation curves from the many-group attenuation curves, we get a set of residual curves. All the residual curves were remarkably close to exponential, accounting in part for the relatively accurate representation of the many-group results by only two effective energies. Fitting each of these residual curves, in turn, by an exponential $B_i^k \exp(-\beta_i^k\ t_i)$, we get 20 sets (B_i^k, β_i^k). In this case, the weights chosen were the reciprocal of the ordinates, i.e.,

$$w_2^k(t_i) = [\tilde{H}_u^k(t_i)]^{-1},$$

where

$$H^k(t_i) = H_u^k(t_i) - A^k \exp(-\hat{\alpha}_i t_i) \tag{14}$$

(the residual values). This weighting scheme minimizes percent error. As was true for the asymptotic exponential, both B_i^k and β_i^k were free parameters. Figure 3 shows a typical asymptotic exponential from the consistent set $(A^k, \hat{\alpha}_i)$ for the higher effective energy, the residual values (plotted with a circle), and the curve $B_i^k \exp(-\beta_i^k t_i)$. The case chosen is the same as for Fig. 2. The same process as that for the asymptotic exponential is repeated, and an average value $\langle \beta_i^k \rangle_k$ is determined from an expression analogous to Eq. (10). A representative energy $\bar{E}_2$ can then in turn be determined. For this energy $\bar{E}_2$, we then get a consistent set of values $\hat{\beta}_i$. By constraining the parameter $\hat{\beta}_i$ and using the same weights $w_2^k(t_i)$, we determine the intercepts $\overset{\circ}{B}{}_i^k$ in a manner exactly analogous to the $\overset{\circ}{A}{}_i^k$. Figure 4 shows a typical fit of the residual curve, continuing the same case as in Figs. 2 and 3. Again exactly analogous to the asymptotic fit, using equations of the same form as Eqs. (11) through (13), we can determine an effective yield at the second effective energy, $\bar{Y}(\bar{E}_2)$, and an intercept parameter, $B^k(\bar{E}_2)$.

The final two-exponential approximation is shown in Fig. 1 for the typical case we have been following, along with a curve for the sum of the exponentials. Figures 5 through 23 give the same information for all the other cases with a sodium capture spectrum. These curves may be compared with the original calculated points for $H_u^k(t_i)$, which are plotted with an asterisk. All of these results are for the uncollided absorbed dose.

C. Comparison of Two-Group Effective Spectra and Many-Group Spectra

Table XV shows a comparison of the uncollided two-group and six-group results for the sample case of a sodium capture spectrum, iron shield, and carbon absorber, where the values given are the ratio

$$R_u^k(t_i) = \frac{H(2\text{-group})}{H(6\text{-group})} = \frac{\sum_{j=1}^{2} \chi_a^k(\bar{E}_j)\ \bar{Y}(\bar{E}_j)\ \exp[-\chi^i(\bar{E}_j)\ t_i]}{\sum_{j=1}^{6} \chi_a^k(E_j)\ Y(E_j)\ \exp[-\chi^i(E_j)\ t_i]} . \tag{15}$$

It is from data such as these that the average absolute deviations and maximum deviations were determined for Tables II through VI. To define these deviations, consider a combination (i,k) and a calculation of R_u^k for N values of areal density $t_{i,\ell}$, as shown in Table XV. The deviation for the ℓth value of t_i, say $t_{i,\ell}$, is then defined as

$$\varepsilon_\ell^{i,k} = R_u^k(t_{i,\ell}) - 1. \tag{16}$$

The average absolute deviation is then defined by

$$\bar{\varepsilon}^{i,k} = \frac{1}{N} \sum_{\ell=1}^{N} |\varepsilon_\ell^{i,k}|, \tag{17}$$

and the maximum deviation by

$$\varepsilon_{max}^{i,k} = \pm \max\left\{ |\varepsilon_\ell^{i,k}| : \ell = 1,2,\ldots,N \right\}, \tag{18}$$

where the sign of $\varepsilon_{max}^{i,k}$ is determined by the sign of the $\varepsilon_\ell^{i,k}$ that corresponds to the maximum $|\varepsilon_\ell^{i,k}|$. Likewise, an overall average absolute deviation is defined by

$$\bar{\varepsilon} = 0.05 \sum_{i,k} \bar{\varepsilon}^{i,k}, \tag{19}$$

and an overall maximum deviation is defined by

$$\varepsilon_{max} = \pm\max\left\{\left|\varepsilon_{max}^{i,k}\right| : \text{all}(i,k)\right\}, \tag{20}$$

where the sign of ε_{max} is determined by the sign of the $\varepsilon_{max}^{i,k}$ that corresponds to the maximum $\left|\varepsilon_{max}^{i,k}\right|$.

It is important to observe that $\bar{\varepsilon}^{i,k}$ is biased toward the $\varepsilon_{\ell}^{i,k}$ for lower values of t_i, because more points were chosen in this region than in the asymptotic region. Table XV is typical of the distribution of the t_i. Also, note that no attempt was made to inroduce a deliberate conservatism into the effective spectra, i.e., to make the effective spectra predict dose rates higher than the many-group spectra. The only bias in the least-squares fit, therefore, was the implicit biasing by the weighting schemes.

As a further comparison of the effective two-group spectra with the many-group spectra, buildup was incorporated in Eq. (15). The form of buildup factor chosen was Taylor's[16] exponential approximation to the moments method data, of the form

$$B(\chi^i\, t_i; E) = C_1(E)\, \exp[-c_1(E)\, \chi^i(E)\, t_i] + C_2(E)\, \exp[-c_2(E)\, \chi^i(E)\, t_i], \tag{21}$$

where

$$C_2 = 1 - C_1.$$

The constants C_ν and c_ν ($\nu = 1,2$) were taken from the tabulation of Guilinger, et al.[6] The equation for the ratio of built-up absorbed doses, corresponding to Eq. (15), is then

$$R^k(t_i) = \frac{\sum_{\nu=1}^{2}\sum_{j=1}^{2} C_\nu(\bar{E}_j)\, \chi_a^k(\bar{E}_j)\, \bar{Y}(\bar{E}_j)\, \exp -[1 + c_\nu(\bar{E}_j)]\, \chi^i(\bar{E}_j)\, t_i}{\sum_{\nu=1}^{2}\sum_{j=1}^{6} C_\nu(E_j)\, \chi_a^k(E_j)\, Y(E_j)\, \exp -[1 + c_\nu(E_j)]\, \chi^i(E_j)\, t_i}. \tag{22}$$

Table XVI presents a comparison using Eq. (22) for our sample case. In this case, the average absolute deviation was lower with buildup than without, viz., 3.31 and 4.19 percent, respectively. However, the maximum deviation, which occurs at the maximum areal density of 500 g/cm^2 for both, is slightly higher with buildup, 13.32 vs 12.49 percent. Average absolute deviation and maximum deviation for Eq. (22) are defined exactly as in Eqs. (17) and (18), with the same biasing of $\bar{\varepsilon}^{i,k}$. It can be noted from Tables II through XI that the average absolute deviation changes only slightly when buildup is incorporated in the comparisons. In fact, the overall average absolute deviation, $\bar{\varepsilon}$, is lower with buildup for nickel and tantalum capture gamma-ray spectra and the prompt fission gamma-ray spectrum. In all cases, incorporating buildup decreased the magnitude of the overall maximum deviation, ε_{max}, for any given source spectrum. The only conclusion that should be drawn from these results is that incorporating buildup did not significantly alter the accuracy of the effective-spectra approximations to the many-group spectra. The changes noted with buildup are within the range one might expect from the errors in the Taylor exponential approximation to the moments data for buildup (p. 73 of Guilinger[6] or pp. 376-378 to Goldstein[7] contain summaries of these errors).

D. Comparison of Previous and Present Effective Spectra for Type 304 Stainless Steel and Prompt Fission

Further comparisons were made between Shure and Strobel's effective spectrum for type 304 stainless steel and the present effective spectrum. These are both two-group effective spectra but were derived using different sources of data for the many-group spectra (see Table XVII), a different assumed composition of type 304 stainless steel, and different combinations of attenuating and absorbing materials. It is thus difficult to separate the causes of discrepancies in calculations using the two different effective spectra. However, as may be noted in Table XVIII, the discrepancies are relatively minor for iron shields, which were used in the

determination of both sets of effective spectra. Table XVIII presents data for the ratio of the present two-group spectrum uncollided dose results to those using Shure and Strobel's effective spectra. Similar results were obtained with built-up absorbed doses. The comparison is good for carbon, sodium, tantalum, and concrete at the lower areal densities. In general, Shure and Strobel used smaller ranges of areal density of attenuating material in determining their effective spectra than did the present study. The new effective spectrum results for type 304 stainless steel would thus be expected to reproduce the many-group spectrum results better at very deep penetrations. This appears to be the case for carbon, sodium, and concrete, where the present effective spectrum predicts dose rates significantly higher than Shure and Strobel's at the deeper penetrations, yet reproduce the six-group results quite well. The closest comparable result of Shure and Strobel's study is for water which has an attenuation coefficient very similar to concrete in the 7 to 8 MeV range. At the deepest penetration in water which they consider, 300 g/cm^2, the ratio of tissue dose using their two-group effective spectrum to that using their ten-group detailed spectrum is 0.791.[5] A similar effect appears in carbon and sodium at penetrations of the order of 300 g/cm^2, indicating that the new effective spectrum may be applicable at deeper penetrations for some of the attenuating materials Shure and Strobel consider.

The comparison of the effective spectra for prompt fission is somewhat more straightforward to analyze, because both spectra are based on the same source spectrum (see Table XVII). As can be seen from Table XVIII, the two effective spectra agree within 11.9 percent over the range of areal density considered. Similar results were obtained for the built-up absorbed doses. This agreement appears to verify the applicability of the three-group effective spectra to attenuating and absorbing materials not used in the determination of the spectra.

REFERENCES

1. P. S. Mittelman and R. A. Liedtke, "Gamma Rays from Thermal-Neutron Capture," Nucleonics 13, No. 5, 50 (May 1955).

2. P. E. Deloume, "Gamma Ray Energy Spectra from Thermal Neutron Capture," APEX-407, General Electric (1958).

3. E. Troubetzkoy and H. Goldstein, "A Compilation of Information on Gamma-Ray Spectra Resulting from Thermal-Neutron Capture," ORNL-2904, Oak Ridge National Laboratory (1961).

4. G. A. Bartholomew and L. A. Higgs, "Compilation of Thermal Neutron Capture Gamma Rays," CRGP-784, Chalk River Project (1958).

5. K. Shure and G. L. Strobel, "Effective Neutron Gapture Gamma Ray Spectra," WAPD-BT-22, Bettis Atomic Power Laboratory (1961).

6. W. H. Guilinger, et al., "SPAN-3, A Shield Design Program for the Philco-2000 Computer," WAPD-TM-235, Bettis Atomic Power Laboratory (1962).

7. H. Goldstein, Fundamental Aspects of Reactor Shielding, Addison-Wesley (1959).

8. 1966 Book of ASTM Standards, Part 1, ASTM Specification A249-65, Am. Soc. for Testing and Materials, Philadelphia, Pa., p. 177.

9. D. J. Hughes and R. B. Schwartz, "Neutron Cross Sections," BNL-325, 2nd ed. (1958) and Supplement I (1960) Brookhaven National Laboratory.

10. F. C. Maienschein, R. W. Peelle, W. Zobel, and T. A. Love, "Gamma Rays Associated with Fission," P/670, Proc. of the Second Int. Conf. on Peaceful Uses of Atomic Energy, Vol. 15, 366 (1958).

11. J. Kirkbride, "The Prompt Gamma Photons from U^{235}, U^{233}, and Pu^{239} Due to the Absorption of a GLEEP Neutron Beam," NRDC-58 (February 1955).

12. Reactor Physics Constants, ANL-5800, 2nd ed., pp. 652-5, Argonne National Laboratory (1963).

13. G. W. Grodstein, "X-Ray Attenuation Coefficients from 10 kev to 100 Mev," NBS Circular 583 (1957).

14. E. Storm, E. Gilbert, and H. Israel, "Gamma-Ray Absorption Coefficients for Elements 1 through 100 Derived from the Theoretical Values of the National Bureau of Standards," LA-2237, Los Alamos Scientific Laboratory (1958).

15. R. H. Moore and R. K. Zeigler, "The Solution of the General Least Squares Problem with Special Reference to High-Speed Computers," LA-2367, Los Alamos Scientific Laboratory (1960).

16. J. J. Taylor, "Applications of Gamma-Ray Buildup Data to Shield Design," WAPD-RM-217, Bettis Atomic Power Laboratory (1954).

TABLE I

Two-Group Effective Gamma-Ray Energies and Energy Yields

	$\bar{E}_j$ Gamma-Ray Energy (MeV)	$\bar{Y}(\bar{E}_j)$ Yield (MeV/capture)
Sodium capture	5.5	6.09
	2.0	5.74
Nickel capture	8.0	8.33
	2.0	1.62
Stainless steel capture	8.0	5.86
	2.0	1.95
Tantalum capture	4.0	3.76
	1.5	2.88
		(MeV/fission)
Prompt fission	4.0	2.31
	1.25	4.92

TABLE II

Comparison of Effective Spectrum and Six-Group Spectrum
Uncollided Calculations for Sodium Capture

Attenuating Material	Maximum Areal Density (g/cm^2)	Absorbing Material	Number of Points	Average Absolute Deviation (%)	Maximum Deviation (%)	Areal Density for Max.Dev. (g/cm^2)
Iron	500	Iron	34	3.73	9.86	460
		Carbon		4.19	12.49	500
		Tantalum		4.05	9.23	420
		Concrete		3.94	11.41	500
		Tissue		4.20	12.34	500
Carbon	300	Iron	24	1.58	- 7.08	300
		Carbon		1.37	4.38	180
		Concrete		1.33	- 4.13	300
		Tissue		1.89	4.52	180
Sodium	260	Iron	22	1.43	3.98	200
		Carbon		1.59	5.51	240
		Tantalum		1.85	4.08	180
		Concrete		1.44	4.79	220
		Tissue		2.10	5.53	240
Tantalum	200	Iron	19	3.19	-13.57	200
		Tantalum		3.15	-12.29	200
Concrete	560	Iron	37	4.74	-22.06	560
		Carbon		3.92	-16.38	560
		Concrete		4.09	-18.58	560
		Tissue		4.27	-16.96	560

Total number of points = 562.
Overall average absolute deviation = 3.14%.

TABLE III

Comparison of Effective Spectrum and Six-Group Spectrum
Uncollided Calculations for Nickel Capture

Attenuating Material	Maximum Areal Density (g/cm^2)	Absorbing Material	Number of Points	Average Absolute Deviation (%)	Maximum Deviation (%)	Areal Density for Max.Dev. (g/cm^2)
Iron	500	Iron	34	2.31	5.97	500
		Carbon		2.92	7.49	500
		Tantalum		2.15	5.38	500
		Concrete		2.22	6.29	500
		Tissue		2.52	6.84	500
Carbon	300	Iron	24	1.86	- 8.16	300
		Carbon		1.19	- 5.22	300
		Concrete		1.52	- 6.94	300
		Tissue		1.25	- 5.93	300
Sodium	300	Iron	24	0.71	- 3.41	300
		Carbon		0.75	1.05	50
		Tantalum		1.13	- 4.46	300
		Concrete		0.50	- 2.43	300
		Tissue		0.53	- 1.55	300
Tantalum	300	Iron	24	2.31	- 8.00	300
		Tantalum		1.81	- 6.48	300
Concrete	560	Iron	37	1.95	- 8.48	560
		Carbon		1.90	- 4.84	560
		Concrete		1.61	- 6.86	560
		Tissue		1.70	- 5.61	560

Total number of points = 582.
Overall average absolute deviation = 1.73%.

TABLE IV

Comparison of Effective Spectrum and Six-Group Spectrum
Uncollided Calculations for Type 304 Stainless Steel Capture

Attenuating Material	Maximum Areal Density (g/cm^2)	Absorbing Material	Number of Points	Average Absolute Deviation (%)	Maximum Deviation (%)	Areal Density for Max.Dev. (g/cm^2)
Iron	500	Iron	34	1.95	6.38	500
		Carbon		2.19	7.38	500
		Tantalum		2.10	6.04	500
		Concrete		1.77	6.39	500
		Tissue		1.94	6.77	500
Carbon	300	Iron	24	1.41	- 6.35	300
		Carbon		0.69	- 3.61	300
		Concrete		1.18	- 5.26	300
		Tissue		0.90	- 4.31	300
Sodium	260	Iron	22	0.24	- 1.13	260
		Carbon		0.58	0.98	220
		Tantalum		0.71	- 1.89	260
		Concrete		0.22	- 0.54	260
		Tissue		0.29	0.62	20,25
Tantalum	300	Iron	24	2.96	-12.17	300
		Tantalum		2.43	-11.19	300
Concrete	560	Iron	37	1.43	- 6.05	560
		Carbon		1.78	3.71	280
		Concrete		1.25	- 4.48	560
		Tissue		1.49	- 3.25	560

Total number of points = 572.
Overall average absolute deviation = 1.46%.

TABLE V

Comparison of Effective Spectrum and Five-Group Spectrum
Uncollided Calculations for Tantalum Capture

Attenuating Material	Maximum Areal Density (g/cm^2)	Absorbing Material	Number of Points	Average Absolute Deviation (%)	Maximum Deviation (%)	Areal Density for Max.Dev. (g/cm^2)
Iron	500	Iron	34	4.26	10.60	420
		Carbon		4.55	12.00	460
		Tantalum		4.40	9.81	400
		Concrete		4.46	11.51	460
		Tissue		4.74	12.25	460
Carbon	300	Iron	24	1.85	5.36	200
		Carbon		2.09	6.20	220
		Concrete		2.02	5.89	220
		Tissue		2.49	6.53	220
Sodium	260	Iron	22	1.88	6.14	240
		Carbon		1.87	7.08	260
		Tantalum		2.37	5.76	220
		Concrete		1.86	6.75	260
		Tissue		2.16	7.40	260
Tantalum	300	Iron	24	5.14	-12.58	300
		Tantalum		3.80	- 9.22	280
Concrete	560	Iron	37	4.89	-24.26	560
		Carbon		4.25	-19.34	560
		Concrete		4.43	-21.05	560
		Tissue		4.48	-19.61	560

Total number of points = 572.
Overall average absolute deviation = 3.62%.

TABLE VI

Comparison of Effective Spectrum and Seven-Group Spectrum
Uncollided Calculations for Prompt Fission

Attenuating Material	Maximum Areal Density (g/cm^2)	Absorbing Material	Number of Points	Average Absolute Deviation (%)	Maximum Deviation (%)	Areal Density for Max.Dev. (g/cm^2)
Iron	400	Iron	29	5.48	13.04	360
		Carbon		6.45	16.47	400
		Tantalum		4.88	11.09	320
		Concrete		6.08	15.32	380
		Tissue		6.47	16.92	400
Carbon	300	Iron	24	2.97	-16.07	300
		Carbon		2.80	- 9.02	300
		Concrete		2.69	-11.40	300
		Tissue		2.70	- 9.13	300
Sodium	250	Iron	24	2.39	- 4.39	70
		Carbon		3.36	5.92	235
		Tantalum		1.87	- 2.74	60
		Concrete		2.91	5.13	220
		Tissue		3.25	6.35	235
Tantalum	100	Iron	14	4.40	-14.24	100
		Tantalum		3.66	-10.91	100
Concrete	340	Iron	26	2.87	-10.79	340
		Carbon		3.29	6.74	220
		Concrete		2.98	- 6.20	340
		Tissue		3.24	7.24	220

Total number of points = 493.
Overall average absolute deviation = 3.82%.

TABLE VII

Comparison of Effective Spectrum and Six-Group Spectrum Built-Up Calculations for Sodium Capture

Attenuating Material	Maximum Areal Density (g/cm^2)	Absorbing Material	Number of Points	Average Absolute Deviation (%)	Maximum Deviation (%)	Areal Density for Max.Dev. (g/cm^2)
Iron	500	Iron	34	3.33	13.14	500
		Carbon		3.31	13.32	500
		Tantalum		4.11	13.49	500
		Concrete		3.22	13.25	500
		Tissue		4.88	18.42	500
Carbon	300	Iron	24	1.50	4.50	240
		Carbon		1.82	5.91	260
		Concrete		1.59	5.27	260
		Tissue		2.32	6.40	260
Sodium	260	Iron	22	2.09	8.33	260
		Carbon		1.53	8.21	260
		Tantalum		2.94	8.88	260
		Concrete		1.75	8.26	260
		Tissue		1.77	7.27	260
Tantalum	200	Iron	19	2.64	-12.70	200
		Tantalum		2.97	-12.53	200
Concrete	560	Iron	37	4.36	11.48	320
		Carbon		5.13	13.56	360
		Concrete		4.74	12.64	340
		Tissue		4.09	10.95	340

Total number of points = 562.
Overall average absolute deviation = 3.24%.

TABLE VIII

Comparison of Effective Spectrum and Six-Group Spectrum Built-Up Calculations for Nickel Capture

Attenuating Material	Maximum Areal Density (g/cm^2)	Absorbing Material	Number of Points	Average Absolute Deviation (%)	Maximum Deviation (%)	Areal Density for Max.Dev. (g/cm^2)
Iron	500	Iron	34	2.52	6.40	500
		Carbon		2.39	6.70	500
		Tantalum		2.72	6.38	500
		Concrete		2.13	6.00	500
		Tissue		1.08	3.75	500
Carbon	300	Iron	24	0.93	-3.95	300
		Carbon		0.58	-1.54	300
		Concrete		0.84	-3.06	300
		Tissue		0.86	-2.57	300
Sodium	300	Iron	24	0.86	1.21	200
		Carbon		1.47	2.46	260
		Tantalum		0.78	-1.60	10
		Concrete		0.98	1.34	240
		Tissue		1.61	-2.23	160
Tantalum	300	Iron	24	2.94	6.23	100
		Tantalum		2.11	4.53	120
Concrete	560	Iron	37	1.85	3.63	280
		Carbon		3.06	5.55	320,340
		Concrete		2.14	4.14	300,320
		Tissue		0.88	-2.24	560

Total number of points = 582.
Overall average absolute deviation = 1.71%.

TABLE IX

Comparison of Effective Spectrum and Six-Group Spectrum Built-Up Calculations for Type 304 Stainless Steel Capture

Attenuating Material	Maximum Areal Density (g/cm^2)	Absorbing Material	Number of Points	Average Absolute Deviation (%)	Maximum Deviation (%)	Areal Density for Max.Dev. (g/cm^2)
Iron	500	Iron	34	1.56	5.65	500
		Carbon		1.43	5.21	500
		Tantalum		2.01	5.97	500
		Concrete		1.31	4.82	500
		Tissue		1.11	2.70	500
Carbon	300	Iron	24	0.76	-2.66	300
		Carbon		0.25	-0.60	300
		Concrete		0.69	-1.98	300
		Tissue		0.79	-1.70	300
Sodium	260	Iron	22	0.68	1.32	260
		Carbon		0.98	2.23	260
		Tantalum		0.87	-1.83	10
		Concrete		0.61	1.32	260
		Tissue		1.77	-3.27	160
Tantalum	300	Iron	24	3.55	-7.43	300
		Tantalum		2.53	-6.85	300
Concrete	560	Iron	37	2.13	4.36	320,340
		Carbon		3.25	6.29	380
		Concrete		2.40	4.88	360
		Tissue		1.05	-2.31	140

Total number of points = 572.
Overall average maximum deviation = 1.56%.

TABLE X

Comparison of Effective Spectrum and Five-Group Spectrum Built-Up Calculations for Tantalum Capture

Attenuating Material	Maximum Areal Density (g/cm^2)	Absorbing Material	Number of Points	Average Absolute Deviation (%)	Maximum Deviation (%)	Areal Density for Max.Dev. (g/cm^2)
Iron	500	Iron	34	3.38	11.97	500
		Carbon		3.44	12.54	500
		Tantalum		3.84	11.49	500
		Concrete		3.47	12.39	500
		Tissue		3.62	11.13	500
Carbon	300	Iron	24	2.82	5.53	260
		Carbon		3.10	6.40	300
		Concrete		2.93	6.10	280
		Tissue		1.89	6.50	280
Sodium	260	Iron	22	1.51	4.93	260
		Carbon		1.58	4.53	260
		Tantalum		2.41	5.28	260
		Concrete		1.44	4.71	260
		Tissue		1.56	4.76	260
Tantalum	300	Iron	24	7.36	-19.08	280
		Tantalum		6.43	-15.90	260
Concrete	560	Iron	37	3.10	-11.77	560
		Carbon		3.08	7.41	340
		Concrete		2.99	- 8.89	560
		Tissue		2.93	- 8.28	560

Total number of points = 572.
Overall average absolute deviation = 3.19%.

TABLE XI

Comparison of Effective Spectrum and Seven-Group Spectrum Built-Up Calculations for Prompt Fission

Attenuating Material	Maximum Areal Density (g/cm^2)	Absorbing Material	Number of Points	Average Absolute Deviation (%)	Maximum Deviation (%)	Areal Density for Max.Dev. (g/cm^2)
Iron	400	Iron	29	4.41	15.10	400
		Carbon		5.12	15.55	400
		Tantalum		4.13	14.67	400
		Concrete		5.31	15.55	400
		Tissue		4.94	14.79	400
Carbon	300	Iron	24	2.79	- 4.93	90
		Carbon		3.32	- 5.96	100
		Concrete		2.56	4.79	260
		Tissue		2.26	5.20	260
Sodium	250	Iron	24	2.64	- 6.39	115
		Carbon		3.27	- 8.03	130
		Tantalum		2.86	- 4.52	100
		Concrete		3.13	- 6.80	130
		Tissue		2.59	- 5.86	130
Tantalum	100	Iron	14	3.78	-14.61	100
		Tantalum		3.10	-12.37	100
Concrete	340	Iron	26	2.66	- 5.83	120
		Carbon		3.63	7.47	300
		Concrete		3.49	6.74	300
		Tissue		2.90	5.96	300

Total number of points = 493.
Overall average absolute deviation = 3.51%.

TABLE XII

Many-Group Capture and Prompt Fission Gamma-Ray Spectra

Group	Energy Range[a] (MeV)	$Y(E_j)$ MeV/capture — Capture Material: Sodium[b]	Chromium	Iron	Nickel[c]	Type 304 Stainless Steel	Tantalum[d]
1	0-1	0.806	0.425	0.375	0.42	0.392	1.03
2	1-2	1.90	0.615	0.96	0.60	0.832	1.48
3	2-3	4.63	0.525	0.675	0.575	0.628	1.65
4	3-5	2.63	0.48	0.867	0.92	0.791	2.20
5	5-7	1.89	1.39	1.50	2.11	1.56	0.275
6	7-9+	0.0	3.82	3.11	5.31	3.59	---
	Total energy	11.86	7.26	7.49	9.94	7.80	6.64
	Binding energy	6.96	9.22	7.65	8.87	----	6.03

		$Y(E_j)$ MeV/fission — Prompt Fission
1	0.3-1	2.62
2	1-2	2.28
3	2-3	1.30
4	3-4	0.610
5	4-5	0.263
6	5-6	0.107
7	6-7	0.0423
	Total energy	7.22

(a) The upper energy of the group, E_j, is used to determine the attenuation and absorption coefficient for that group.
(b) Includes ^{24}Na decay gamma rays (4.12 MeV).
(c) Includes ^{65}Ni decay gamma rays.
(d) Includes ^{182m}Ta decay gamma rays.

TABLE XIII

Comparison of Effective Spectrum and Many-Group Spectrum
Uncollided Calculations for Five Cases Not Used in the Weighting Process

Source Spectrum	Attenuating Material	Maximum Areal Density (g/cm^2)	Absorbing Material	Number of Points	Average Absolute Deviation (%)	Maximum Deviation (%)	Areal Density for Max.Dev. (g/cm^2)
Sodium capture	Carbon	300	Tantalum	24	2.25	- 9.3	300
↓	Tantalum	200	Carbon	19	3.43	-14.79	200
↓	↓	↓	Concrete	19	3.31	-14.14	200
↓	↓	↓	Tissue	19	3.41	-13.28	200
↓	Concrete	560	Tantalum	37	5.72	-24.75	560
Nickel capture	Carbon	300	Tantalum	24	2.50	- 9.39	300
↓	Tantalum	↓	Carbon	24	3.15	-10.49	300
↓	↓	↓	Concrete	24	2.70	- 9.84	300
↓	↓	↓	Tissue	24	3.02	-10.06	300
↓	Concrete	560	Tantalum	37	2.31	-10.01	560
304 Stainless	Carbon	300	Tantalum	24	2.20	- 7.49	300
steel capture	Tantalum	↓	Carbon	24	3.85	-13.68	300
↓	↓	↓	Concrete	24	3.43	-13.31	300
↓	↓	↓	Tissue	24	3.74	-13.14	300
↓	Concrete	560	Tantalum	37	1.69	- 7.55	560
Tantalum capture	Carbon	300	Tantalum	24	2.09	5.07	180
↓	Tantalum	↓	Carbon	24	6.44	-16.19	300
↓	↓	↓	Concrete	24	6.05	-14.97	300
↓	↓	↓	Tissue	24	6.22	-15.30	300
↓	Concrete	560	Tantalum	37	5.88	-27.95	560
Prompt fission	Carbon	300	Tantalum	24	3.62	-21.10	300
↓	Tantalum	100	Carbon	14	5.04	-16.11	100
↓	↓	↓	Concrete	14	5.02	-14.76	100
↓	↓	↓	Tissue	14	4.93	-15.52	100
↓	Concrete	340	Tantalum	26	3.16	-15.78	340

TABLE XIV

Comparison of Effective Spectrum and Many-Group Spectrum
Built-Up Calculations for Five Cases Not Used in the Weighting Process

Source Spectrum	Attenuating Material	Maximum Areal Density (g/cm^2)	Absorbing Material	Number of Points	Average Absolute Deviation (%)	Maximum Deviation (%)	Areal Density for Max.Dev. (g/cm^2)
Sodium capture	Carbon	300	Tantalum	24	2.02	4.75	220
↓	Tantalum	200	Carbon	19	2.90	-12.63	200
↓	↓	↓	Concrete	19	2.84	-12.39	200
↓	↓	↓	Tissue	19	3.49	-11.05	200
↓	Concrete	560	Tantalum	37	4.73	11.36	300
Nickel capture	Carbon	300	Tantalum	24	1.52	- 4.95	300
↓	Tantalum	↓	Carbon	24	4.14	8.59	100
↓	↓	↓	Concrete	24	3.59	7.49	100
↓	↓	↓	Tissue	24	4.15	8.73	100
↓	Concrete	560	Tantalum	37	1.70	- 3.27	560
304 Stainless	Carbon	300	Tantalum	24	1.38	- 3.50	300
steel capture	Tantalum	↓	Carbon	24	5.03	9.65	100
↓	↓	↓	Concrete	24	4.41	8.42	100
↓	↓	↓	Tissue	24	5.13	9.94	100
↓	Concrete	560	Tantalum	37	1.88	3.78	300
Tantalum capture	Carbon	300	Tantalum	24	3.36	5.24	240
↓	Tantalum	↓	Carbon	24	8.45	-22.37	280
↓	↓	↓	Concrete	24	8.13	-21.25	280
↓	↓	↓	Tissue	24	8.35	-21.51	280
↓	Concrete	560	Tantalum	37	3.88	-15.14	560
Prompt fission	Carbon	300	Tantalum	24	3.16	- 4.66	25
↓	Tantalum	100	Carbon	14	4.31	-14.79	100
↓	↓	↓	Concrete	14	4.78	-13.65	100
↓	↓	↓	Tissue	14	4.41	-14.32	100
↓	Concrete	340	Tantalum	26	2.69	4.36	260

TABLE XV

Uncollided Absorbed Dose

Spectrum	Shield Material	Absorption Material
Sodium Capture	Iron	Carbon

Shield Thickness (g/cm^2)	H(2-group)/H(6-group)
0	0.9971
5	0.9984
10	0.9991
15	0.9992
20	0.9988
25	0.9980
30	0.9968
40	0.9938
50	0.9904
60	0.9868
70	0.9835
80	0.9807
90	0.9784
100	0.9769
120	0.9763
140	0.9787
160	0.9841
180	0.9918
200	1.0015
220	1.0124
240	1.0242
260	1.0364
280	1.0485
300	1.0603
320	1.0715
340	1.0818
360	1.0912
380	1.0995
400	1.1067
420	1.1127
440	1.1175
460	1.1211
480	1.1235
500	1.1249

Number of cases = 34.
Total deviation = 1.4245.
Average deviation = 0.0419.
Maximum deviation = 0.1249.

TABLE XVI

Built-Up Absorbed Dose

Spectrum	Shield Material	Absorption Material
Sodium Capture	Iron	Carbon

Shield Thickness (g/cm^2)	H(2-group)/H(6-group)
0	0.9971
5	0.9932
10	0.9924
15	0.9933
20	0.9949
25	0.9968
30	0.9987
40	1.0015
50	1.0027
60	1.0021
70	1.0000
80	0.9965
90	0.9921
100	0.9872
120	0.9768
140	0.9675
160	0.9607
180	0.9570
200	0.9567
220	0.9598
240	0.9660
260	0.9748
280	0.9858
300	0.9985
320	1.0124
340	1.0271
360	1.0421
380	1.0571
400	1.0718
420	1.0860
440	1.0993
460	1.1117
480	0.1230
500	1.1332

Number of cases = 34.
Total deviation = 1.1243.
Average deviation = 0.0331.
Maximum deviation = 0.1332.

TABLE XVII

Gamma-Ray Energy Yields for Many-Group Spectra
(MeV/capture)

Energy Range (MeV)	Type 304 Stainless Steel			Prompt Fission	
	Shure & Strobel		This Report	Shure & Strobel	This Report
0-1	1.11		0.392	2.62[(a)]	2.62
1-2	0.896		0.832	2.26	2.28
2-3	0.171		0.628	1.30	1.30
3-4	0.338	0.824	0.791	0.61	0.610
4-5	0.486			0.26	0.263
5-6	0.964	1.617	1.56	0.11	0.107
6-7	0.653			0.04	0.0423
7-8	2.17	3.564	3.59		
8-9	1.17				
9-10	0.224				

(a) Shure and Strobel break this group into four subgroups: 0-0.4, 0.4-0.6, 0.6-0.8, and 0.8-1.0 MeV.

TABLE XVIII

Comparison of Uncollided Doses Using Two Different Effective Spectra for 304 Stainless Steel and for Prompt Fission

Spectrum	Attenuating Material	Maximum Areal Density (g/cm^2)	Average Absolute Deviation[a] (%)	Maximum Deviation[b] (%)	Absorbing Material with Max. Dev.	Areal Density for Max.Dev. (g/cm^2)
304 Stainless steel	Iron	480	2.7	- 9.8	Carbon	0
	Carbon	200	5.7	21.7	Iron	200
	Sodium	200	4.8	14.91	Iron	200
	Tantalum	300	3.8	-10.9	Tantalum	300
	Concrete	300	9.5	35.5	Iron	300
Prompt fission	Iron	480	4.6	11.9	Tantalum	480
	Carbon	300	3.5	11.3	Iron	300
	Sodium	300	3.4	10.7	Tantalum	300
	Tantalum	100	2.6	-10.0	Iron	100
	Concrete	300	3.3	10.5	Iron	300

(a) Average absolute deviation here is defined by

$$\frac{1}{N(i)} \sum_{k=1}^{N(i)} \bar{\epsilon}^{i,k}.$$

(b) Maximum deviation here is defined by $\pm\max\{|\epsilon^{i,k}_{max}| : k=1,2,\ldots,N(i)\}$.

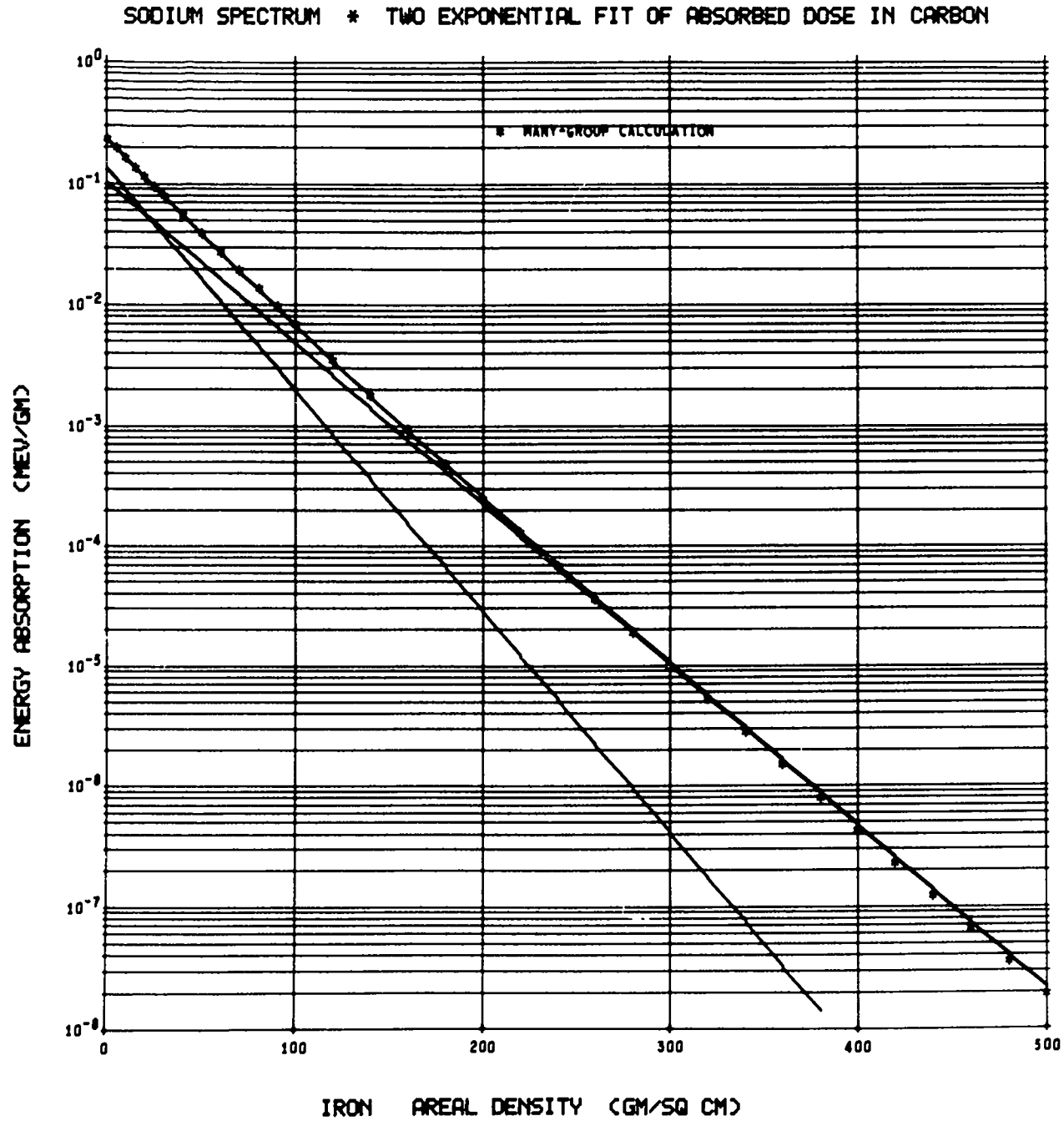
SODIUM SPECTRUM * TWO EXPONENTIAL FIT OF ABSORBED DOSE IN CARBON
* MANY-GROUP CALCULATION
ENERGY ABSORPTION (MEV/GM)
IRON AREAL DENSITY (GM/SQ CM)
10^0
10^-1
10^-2
10^-3
10^-4
10^-5
10^-6
10^-7
10^-8
0
100
200
300
400
500

Fig. 1

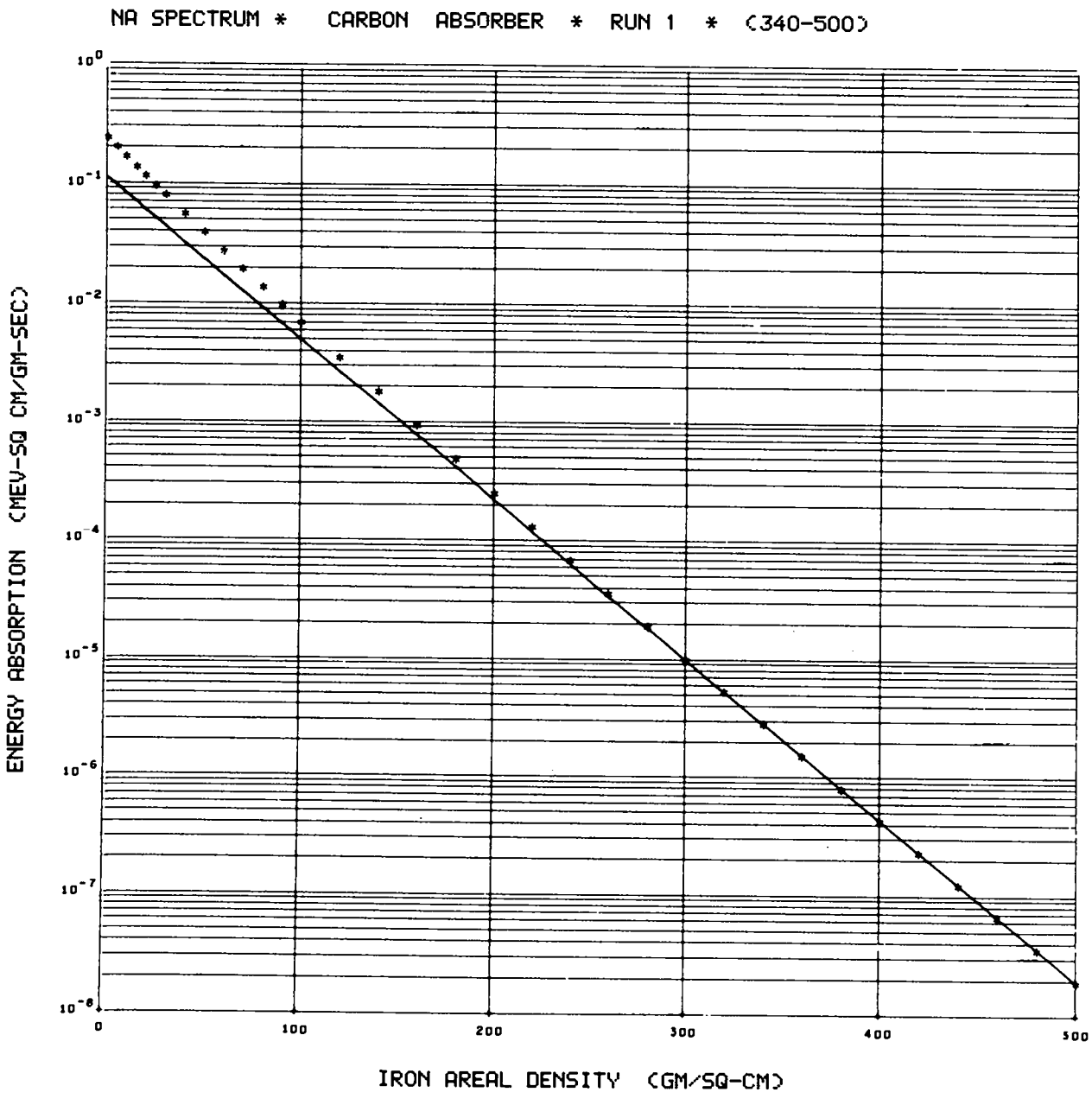
NA SPECTRUM * CARBON ABSORBER * RUN 1 * (340-500)
ENERGY ABSORPTION (MEV-SQ CM/GM-SEC)
IRON AREAL DENSITY (GM/SQ-CM)
10^0
10^-1
10^-2
10^-3
10^-4
10^-5
10^-6
10^-7
10^-8
0
100
200
300
400
500

Fig. 2

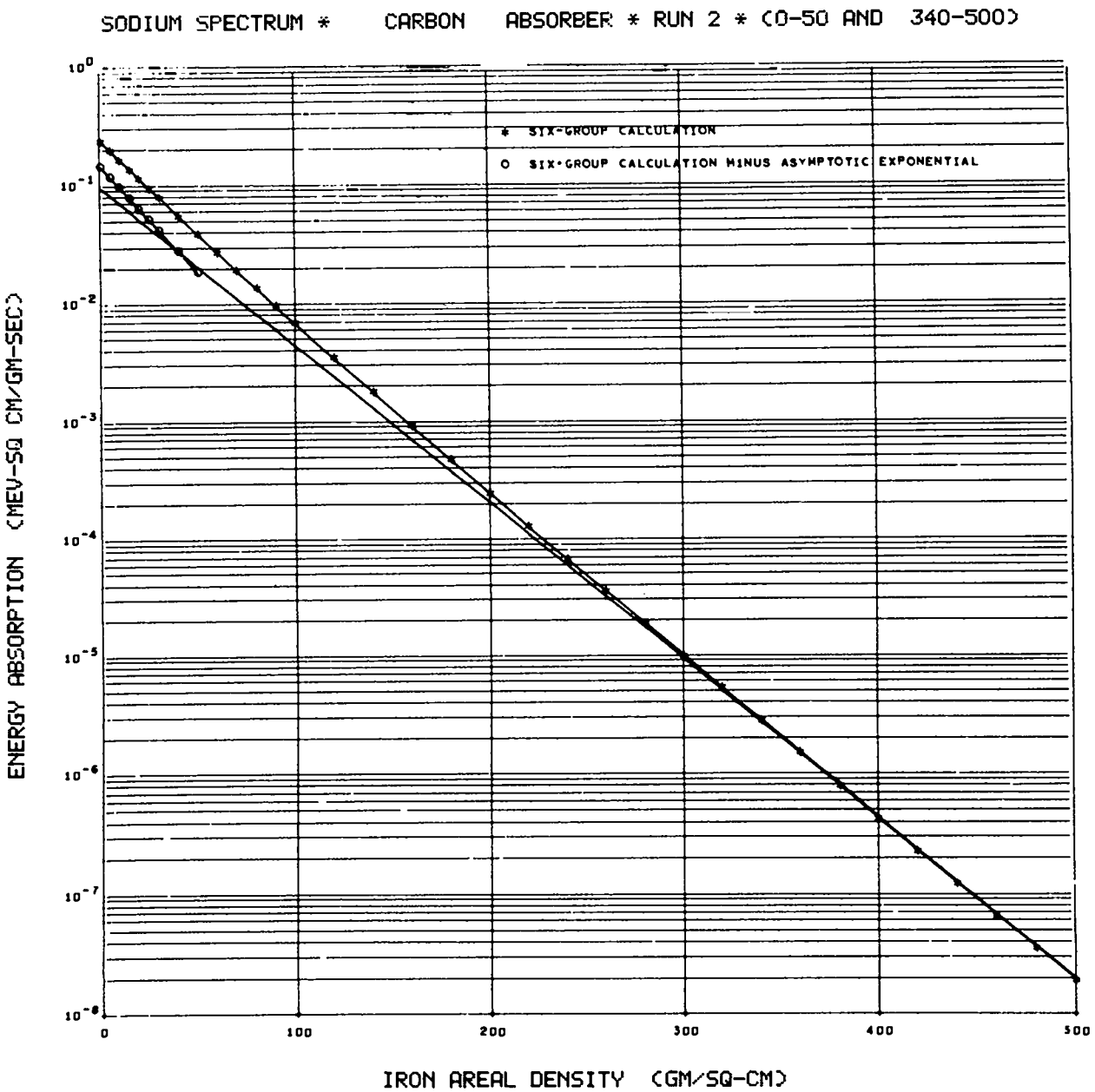
SODIUM SPECTRUM * CARBON ABSORBER * RUN 2 * (0-50 AND 340-500)
* SIX-GROUP CALCULATION
O SIX-GROUP CALCULATION MINUS ASYMPTOTIC EXPONENTIAL
ENERGY ABSORPTION (MEV-SQ CM/GM-SEC)
IRON AREAL DENSITY (GM/SQ-CM)
10^0
10^-1
10^-2
10^-3
10^-4
10^-5
10^-6
10^-7
10^-8
0
100
200
300
400
500

Fig. 3

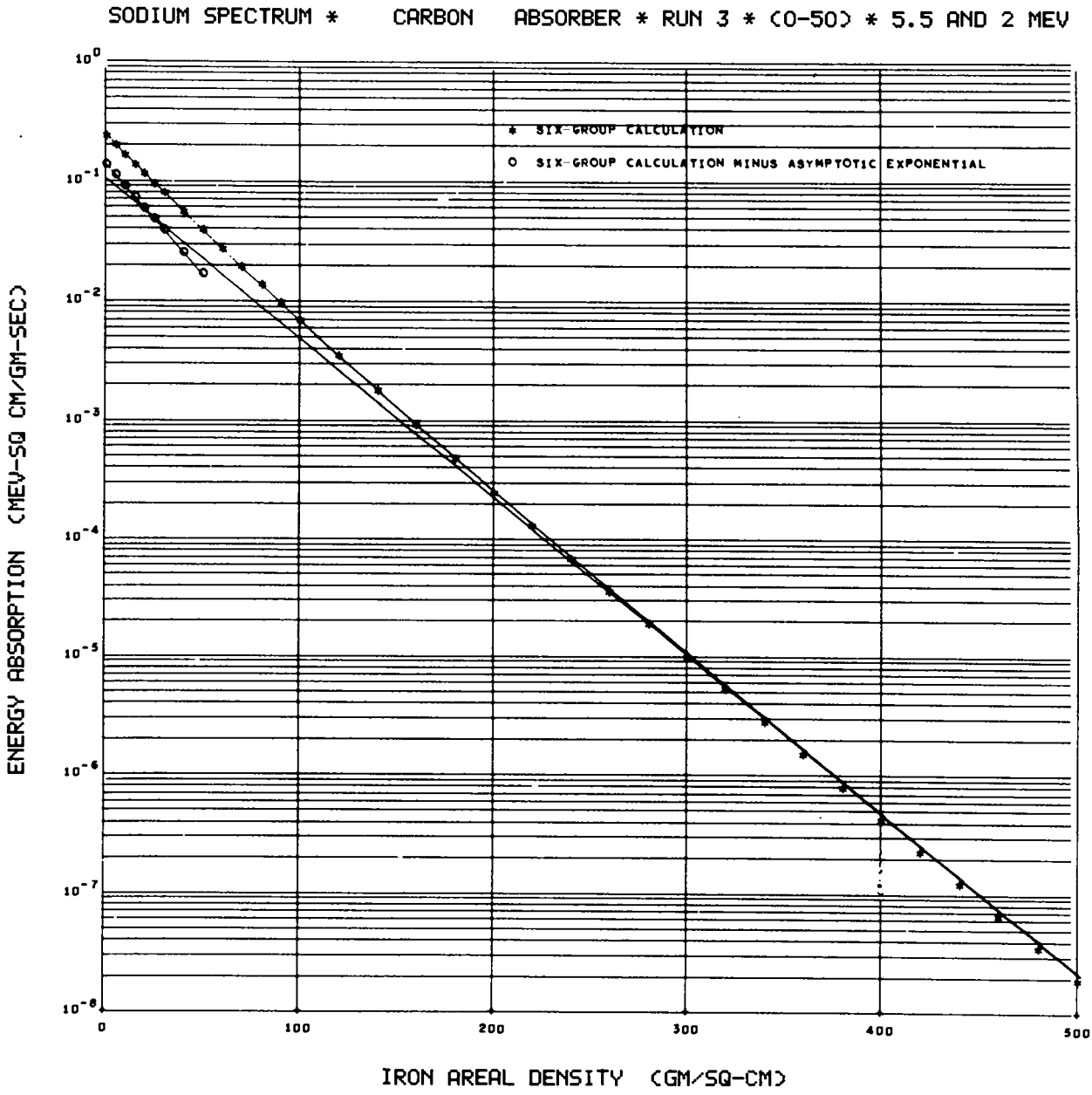
SODIUM SPECTRUM * CARBON ABSORBER * RUN 3 * (0-50) * 5.5 AND 2 MEV
* SIX-GROUP CALCULATION
O SIX-GROUP CALCULATION MINUS ASYMPTOTIC EXPONENTIAL
ENERGY ABSORPTION (MEV-SQ CM/GM-SEC)
IRON AREAL DENSITY (GM/SQ-CM)
10^0
10^-1
10^-2
10^-3
10^-4
10^-5
10^-6
10^-7
10^-8
0
100
200
300
400
500

Fig. 4

SODIUM SPECTRUM * TWO EXPONENTIAL FIT OF ABSORBED DOSE IN IRON
* MANY-GROUP CALCULATION
ENERGY ABSORPTION (MEV/GM)
IRON AREAL DENSITY (GM/SQ CM)
10^0
10^-1
10^-2
10^-3
10^-4
10^-5
10^-6
10^-7
10^-8
0
100
200
300
400
500

Fig. 5

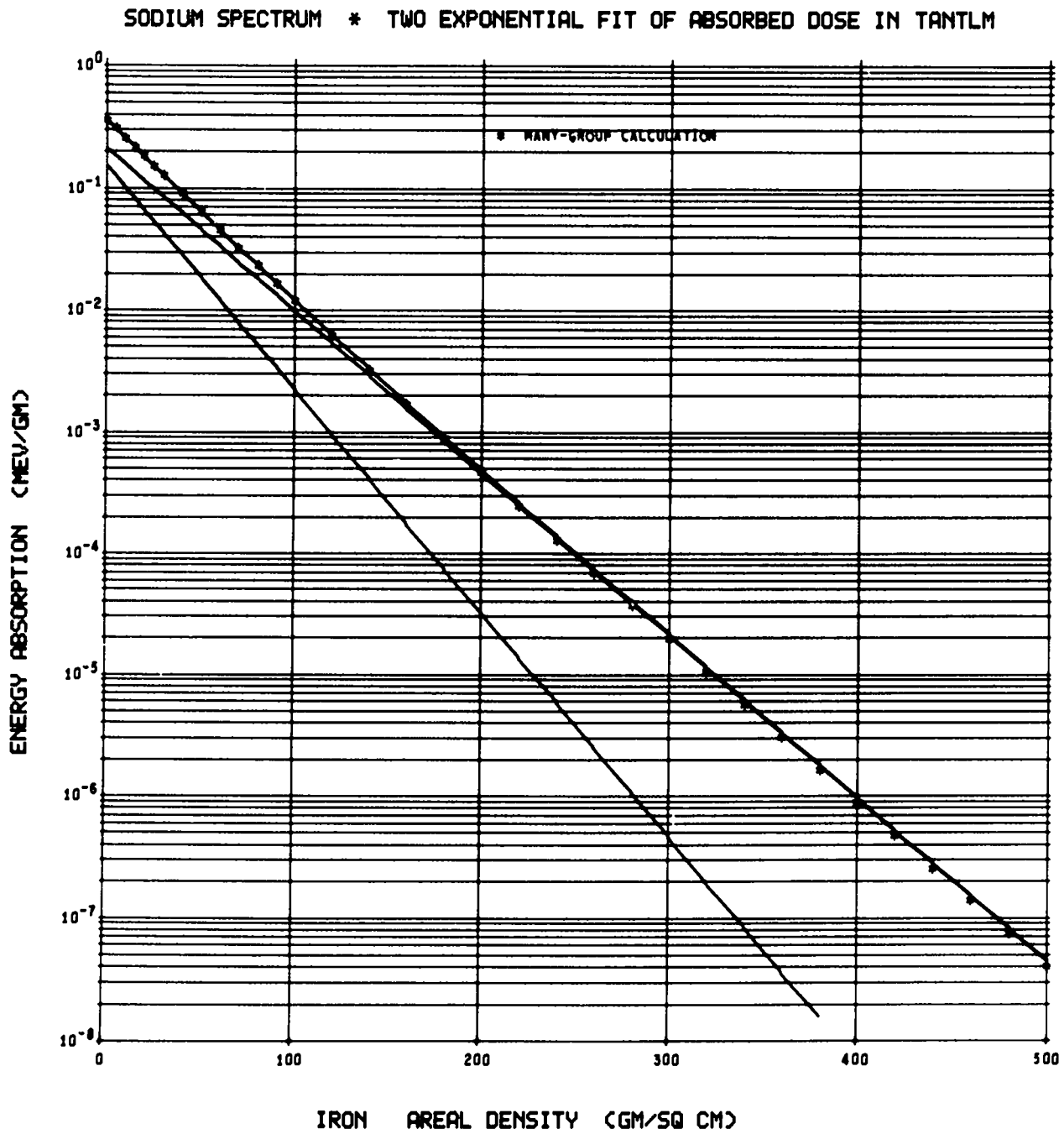
SODIUM SPECTRUM * TWO EXPONENTIAL FIT OF ABSORBED DOSE IN TANTLM
* MANY-GROUP CALCULATION
ENERGY ABSORPTION (MEV/GM)
IRON AREAL DENSITY (GM/SQ CM)
10^0
10^-1
10^-2
10^-3
10^-4
10^-5
10^-6
10^-7
10^-8
0
100
200
300
400
500

Fig. 6

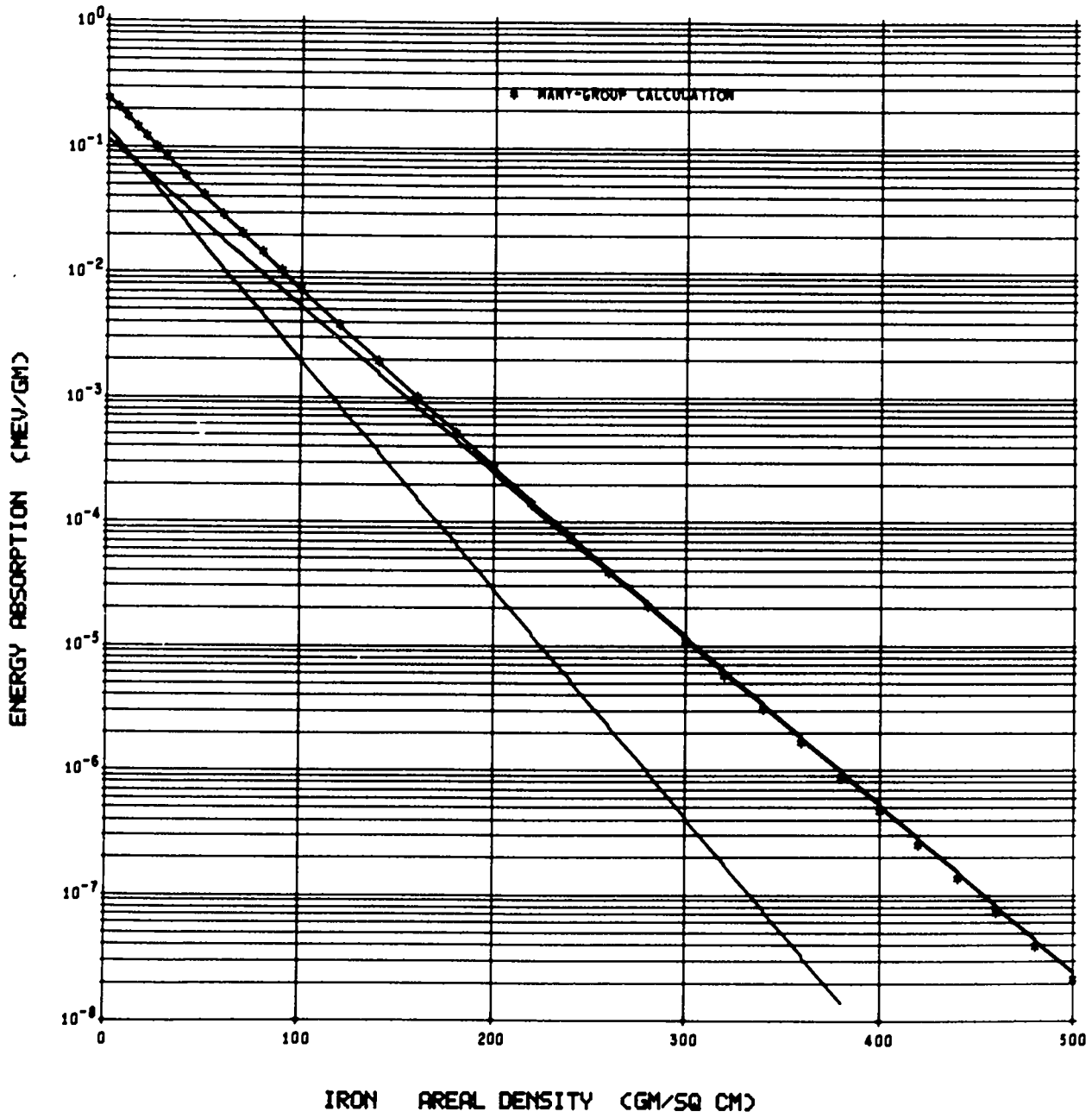
SODIUM SPECTRUM * TWO EXPONENTIAL FIT OF ABSORBED DOSE IN CONCRT
* MANY-GROUP CALCULATION
ENERGY ABSORPTION (MEV/GM)
10^{0}
10^{-1}
10^{-2}
10^{-3}
10^{-4}
10^{-5}
10^{-6}
10^{-7}
10^{-8}
0
100
200
300
400
500
IRON AREAL DENSITY (GM/SQ CM)

Fig. 7

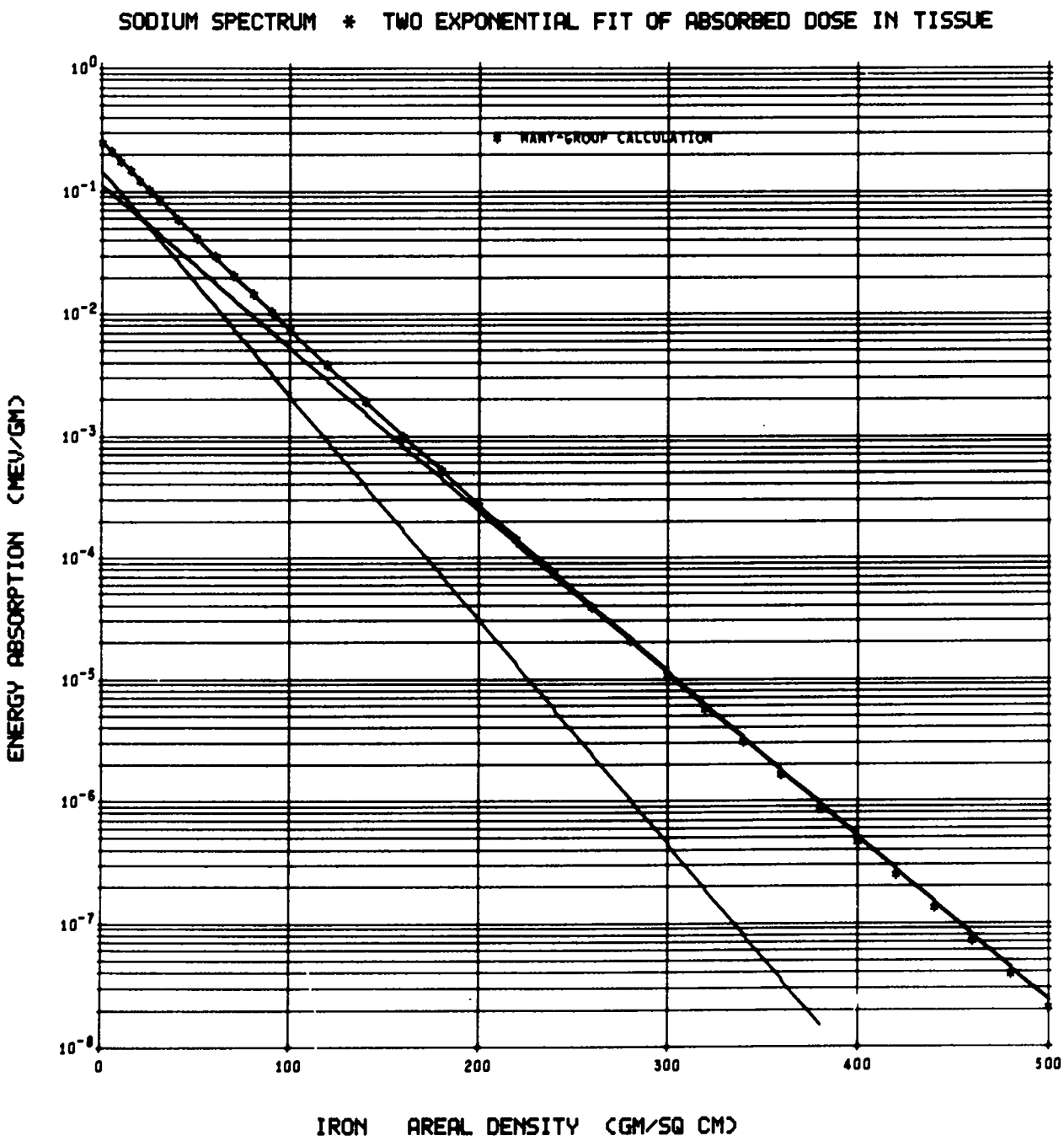
SODIUM SPECTRUM * TWO EXPONENTIAL FIT OF ABSORBED DOSE IN TISSUE
* MANY-GROUP CALCULATION
ENERGY ABSORPTION (MEV/GM)
IRON AREAL DENSITY (GM/SQ CM)
10^0
10^-1
10^-2
10^-3
10^-4
10^-5
10^-6
10^-7
10^-8
0
100
200
300
400
500

FIG. 8

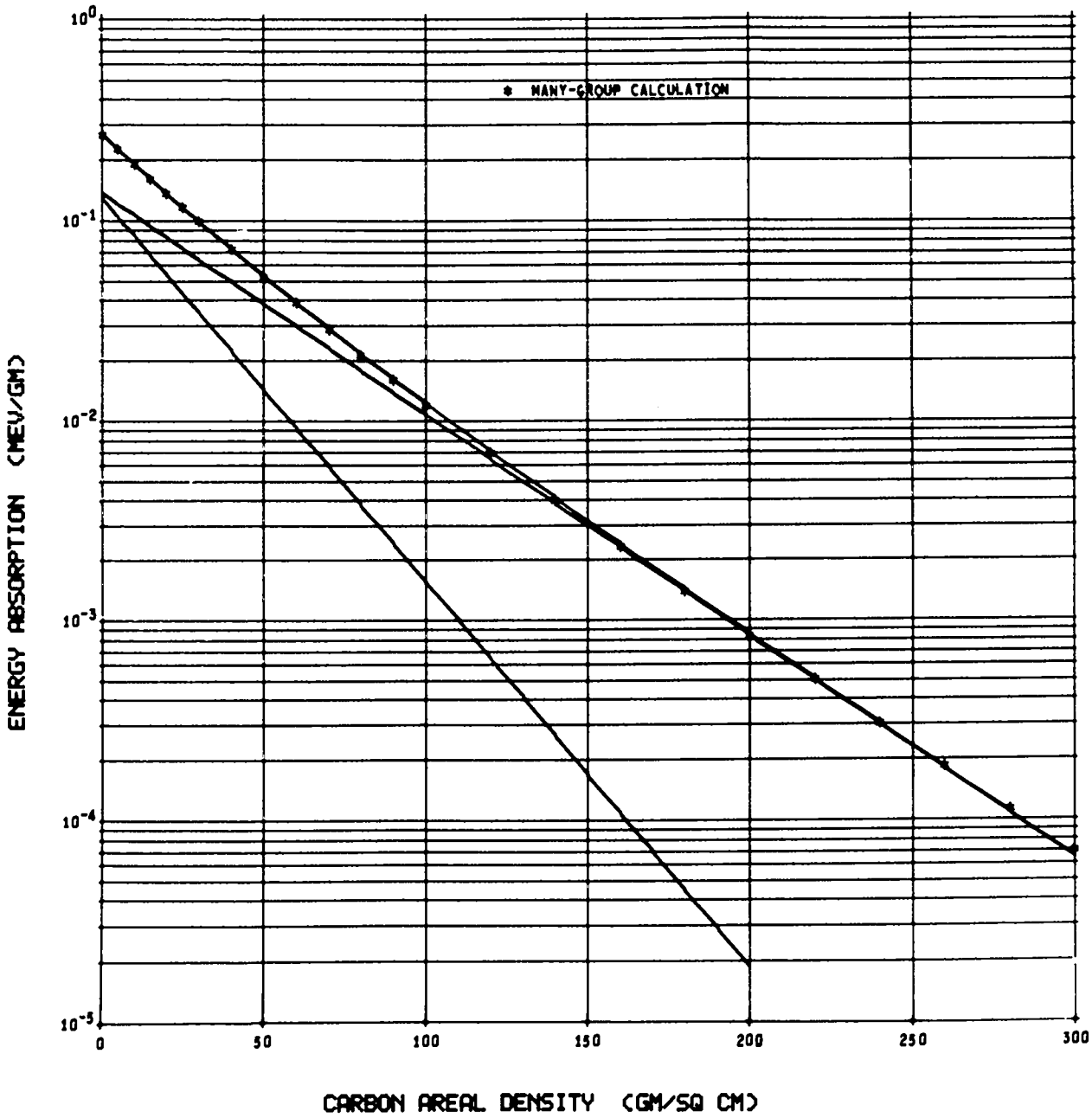
SODIUM SPECTRUM * TWO EXPONENTIAL FIT OF ABSORBED DOSE IN IRON
* MANY-GROUP CALCULATION
ENERGY ABSORPTION (MEV/GM)
CARBON AREAL DENSITY (GM/SQ CM)
10^{0}
10^{-1}
10^{-2}
10^{-3}
10^{-4}
10^{-5}
0
50
100
150
200
250
300

Fig. 9

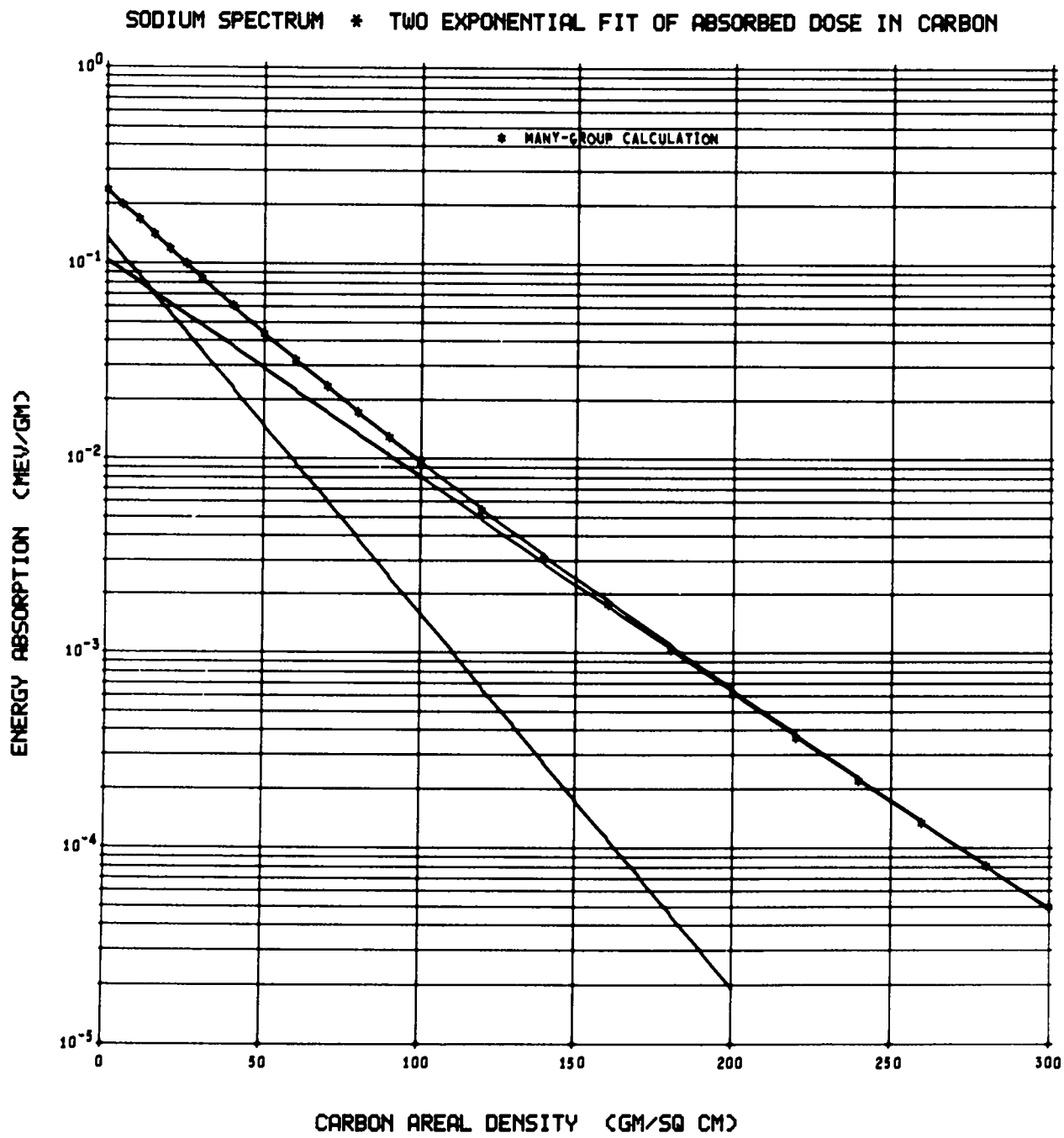
SODIUM SPECTRUM * TWO EXPONENTIAL FIT OF ABSORBED DOSE IN CARBON
* MANY-GROUP CALCULATION
ENERGY ABSORPTION (MEV/GM)
CARBON AREAL DENSITY (GM/SQ CM)
10^0
10^-1
10^-2
10^-3
10^-4
10^-5
0
50
100
150
200
250
300

Fig. 10

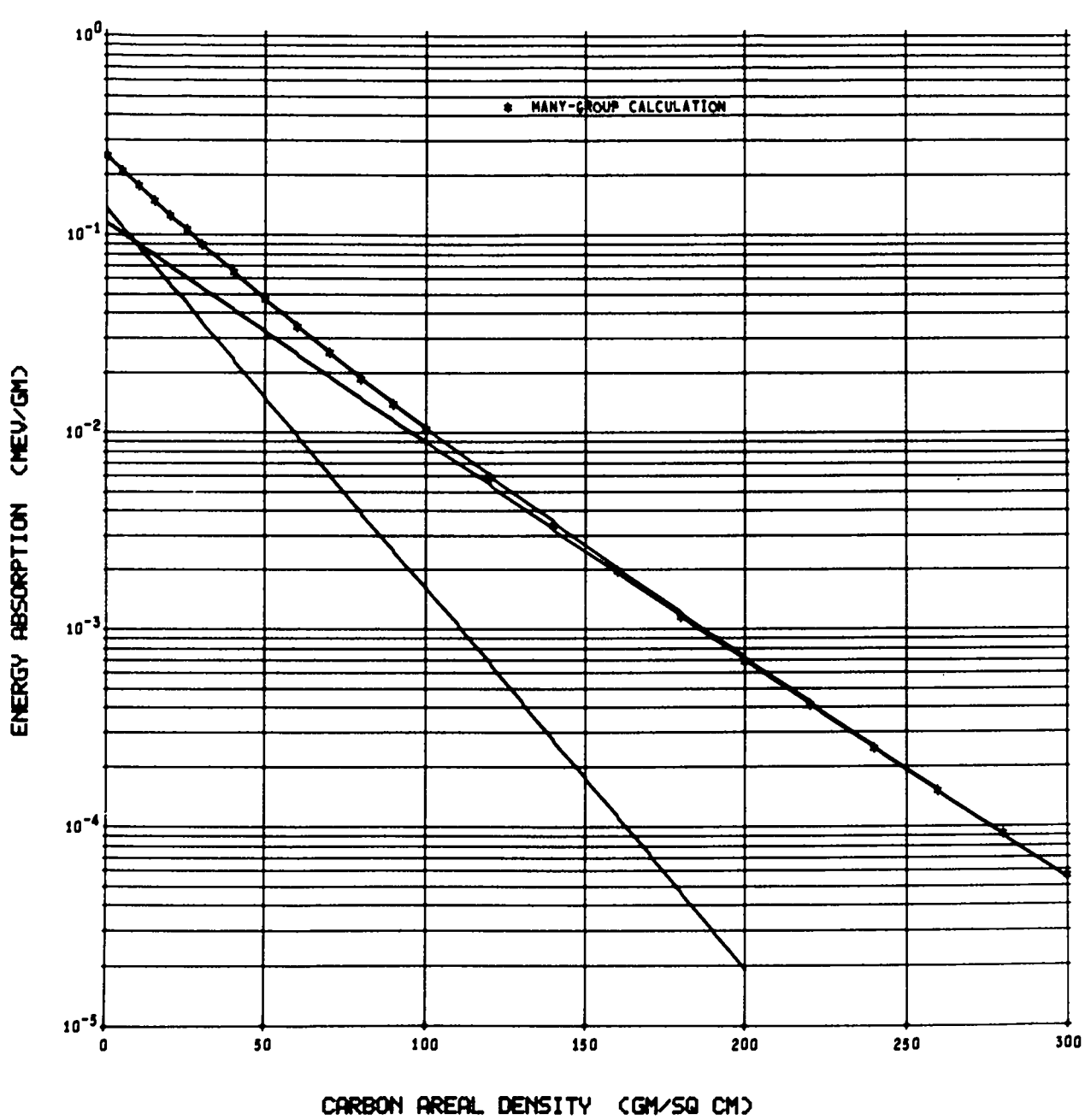
SODIUM SPECTRUM * TWO EXPONENTIAL FIT OF ABSORBED DOSE IN CONCRT
* MANY-GROUP CALCULATION
ENERGY ABSORPTION (MEV/GM)
CARBON AREAL DENSITY (GM/SQ CM)
10^0
10^-1
10^-2
10^-3
10^-4
10^-5
0
50
100
150
200
250
300

Fig. 11

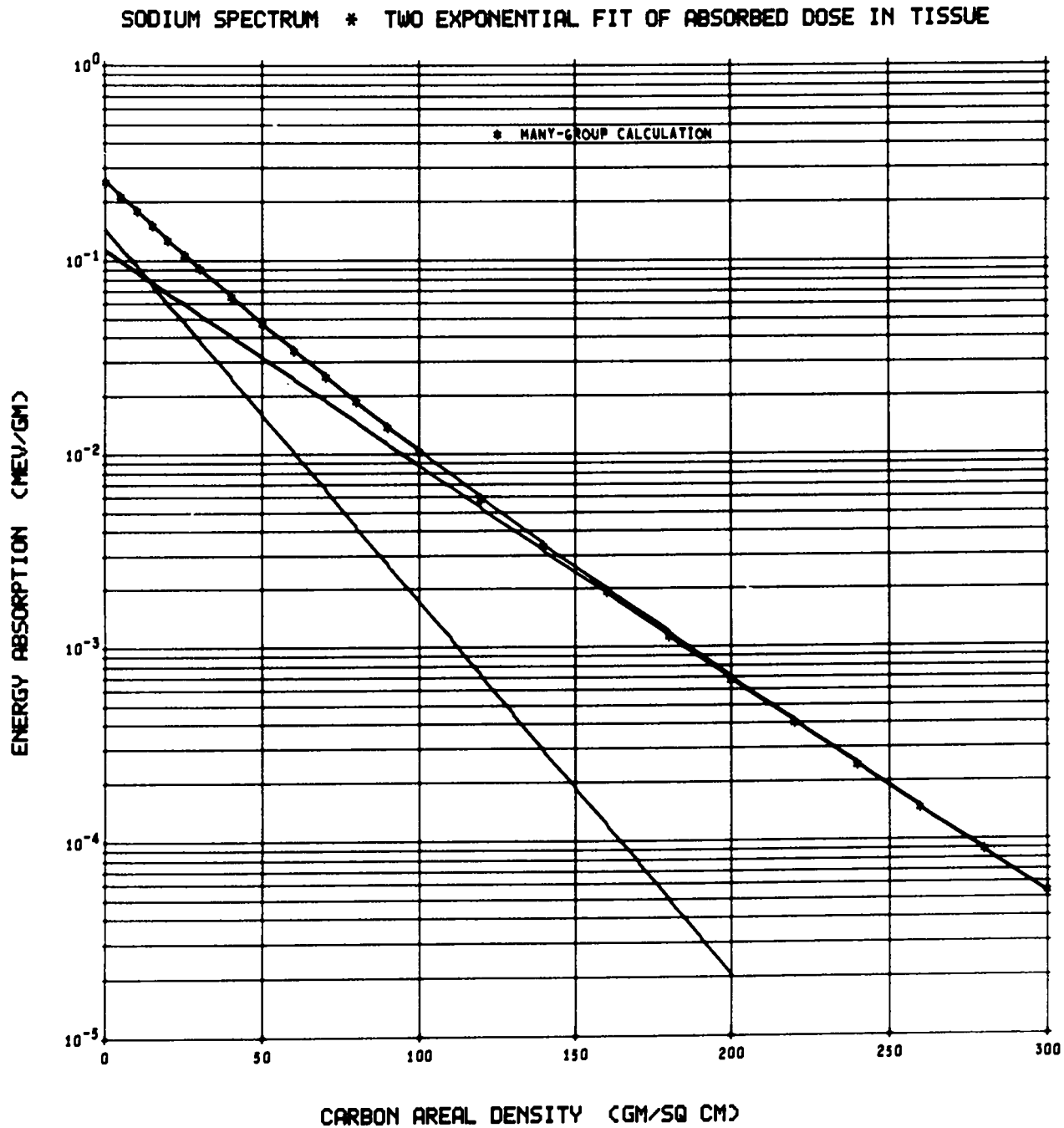
SODIUM SPECTRUM * TWO EXPONENTIAL FIT OF ABSORBED DOSE IN TISSUE
* MANY-GROUP CALCULATION
ENERGY ABSORPTION (MEV/GM)
10^{0}
10^{-1}
10^{-2}
10^{-3}
10^{-4}
10^{-5}
0
50
100
150
200
250
300
CARBON AREAL DENSITY (GM/SQ CM)

Fig. 12

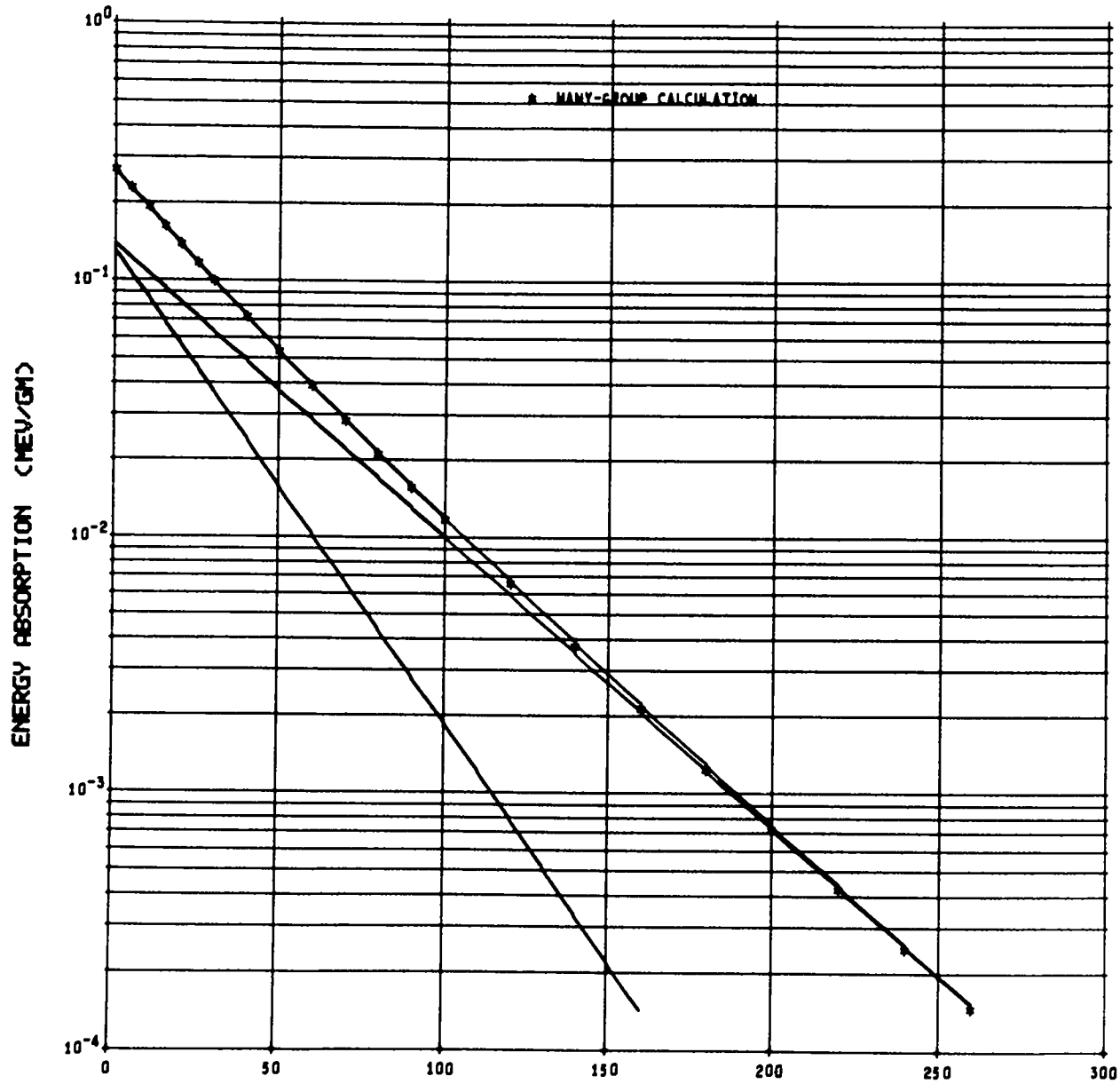
SODIUM SPECTRUM * TWO EXPONENTIAL FIT OF ABSORBED DOSE IN IRON
* MANY-GROUP CALCULATION
ENERGY ABSORPTION (MEV/GM)
10^{0}
10^{-1}
10^{-2}
10^{-3}
10^{-4}
0
50
100
150
200
250
300
SODIUM AREAL DENSITY (GM/SQ CM)

Fig. 13

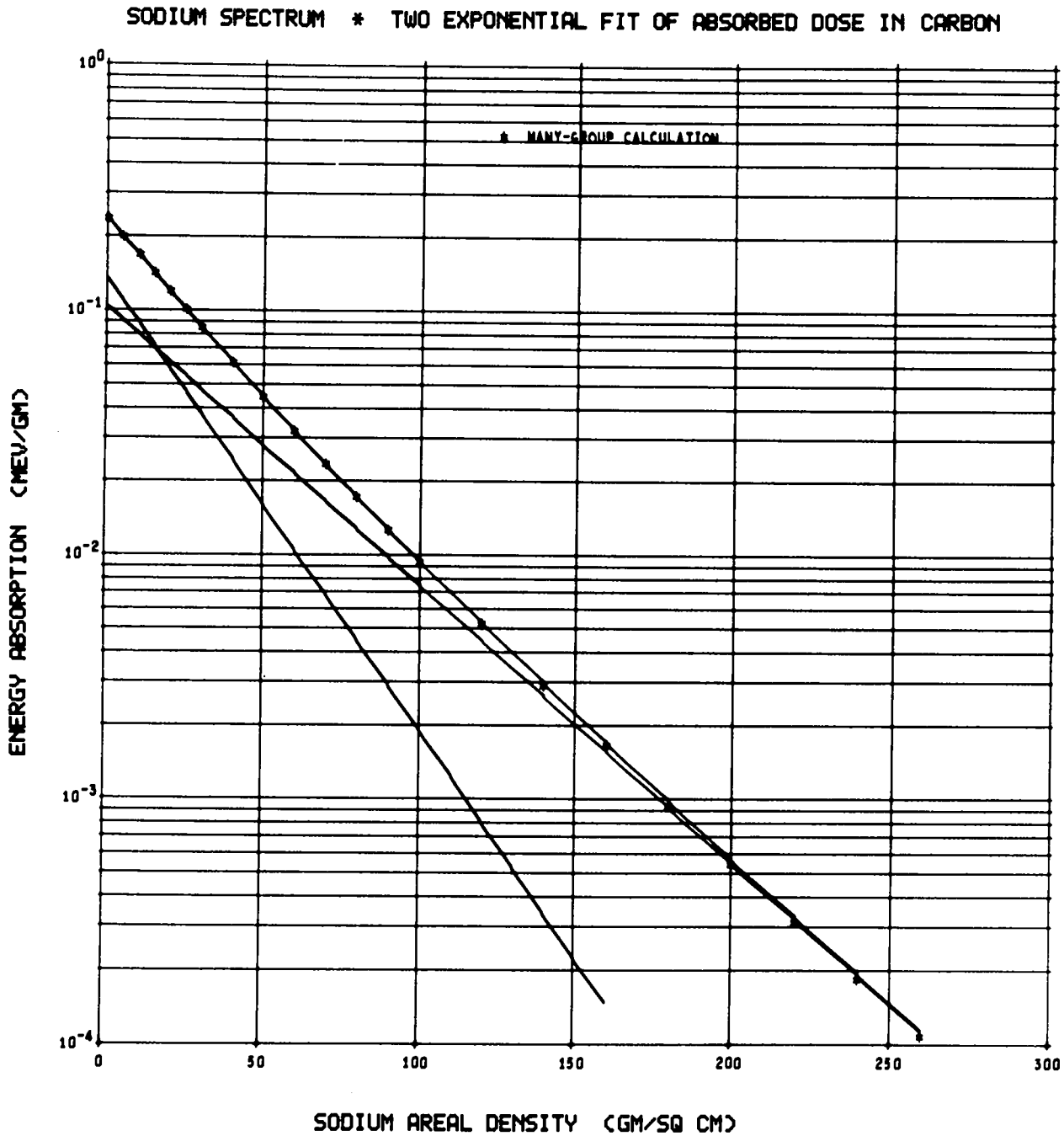
SODIUM SPECTRUM * TWO EXPONENTIAL FIT OF ABSORBED DOSE IN CARBON
* MANY-GROUP CALCULATION
ENERGY ABSORPTION (MEV/GM)
SODIUM AREAL DENSITY (GM/SQ CM)
10^0
10^-1
10^-2
10^-3
10^-4
0
50
100
150
200
250
300

Fig. 14

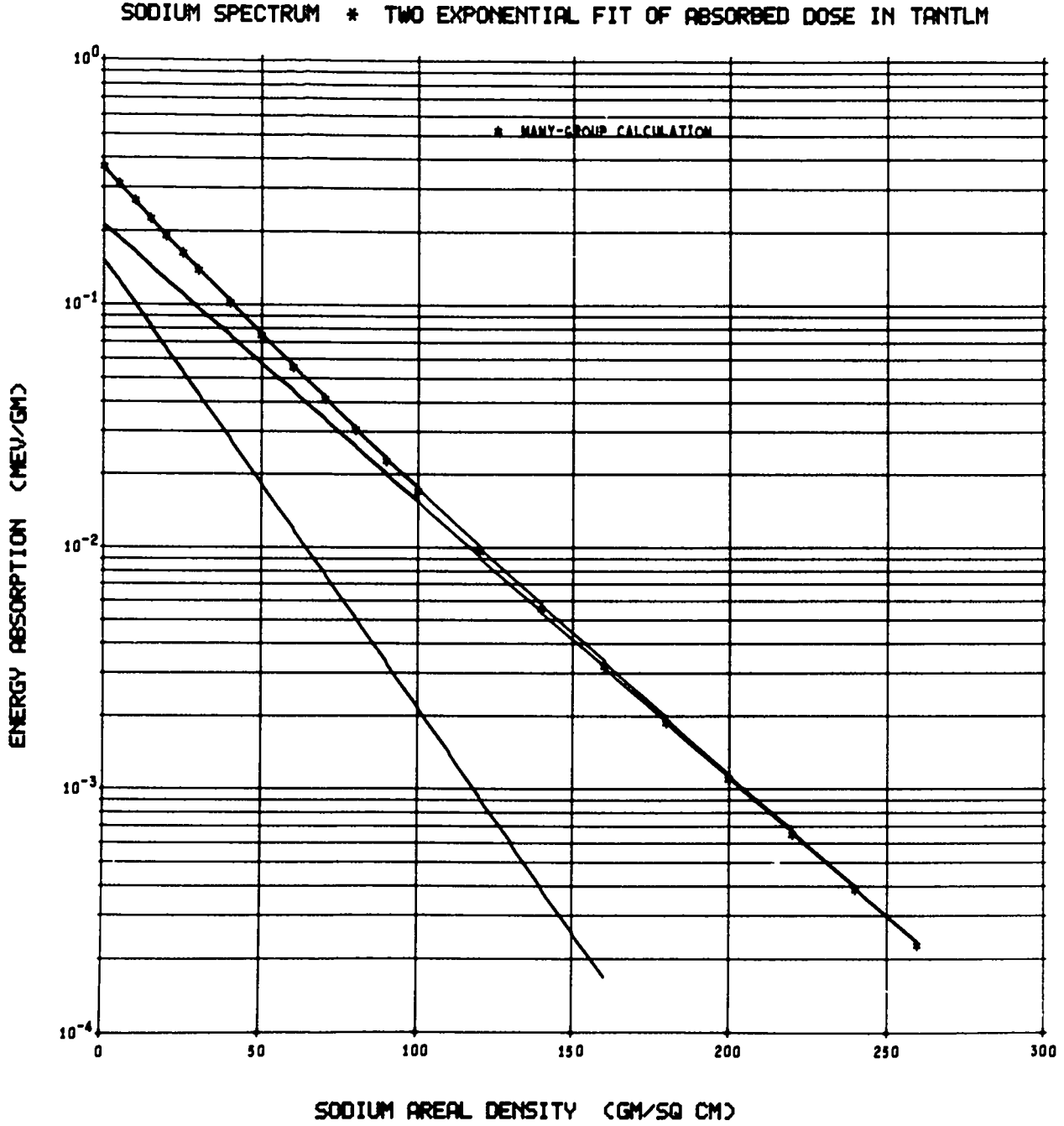
SODIUM SPECTRUM * TWO EXPONENTIAL FIT OF ABSORBED DOSE IN TANTLM
* MANY-GROUP CALCULATION
ENERGY ABSORPTION (MEV/GM)
SODIUM AREAL DENSITY (GM/SQ CM)
10^{0}
10^{-1}
10^{-2}
10^{-3}
10^{-4}
0
50
100
150
200
250
300

Fig. 15

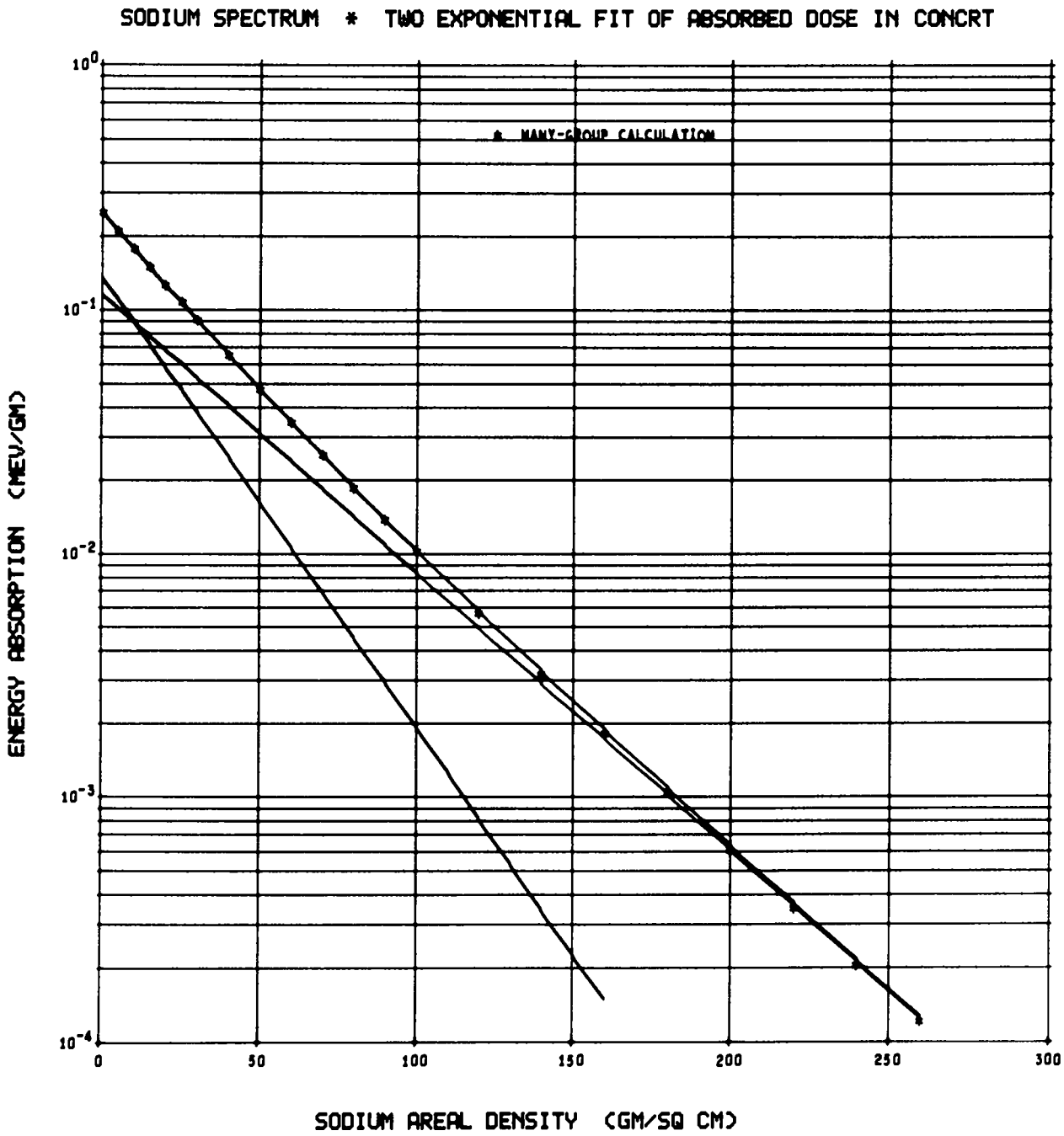
SODIUM SPECTRUM * TWO EXPONENTIAL FIT OF ABSORBED DOSE IN CONCRT
* MANY-GROUP CALCULATION
ENERGY ABSORPTION (MEV/GM)
SODIUM AREAL DENSITY (GM/SQ CM)
10^0
10^-1
10^-2
10^-3
10^-4
0
50
100
150
200
250
300

Fig. 16

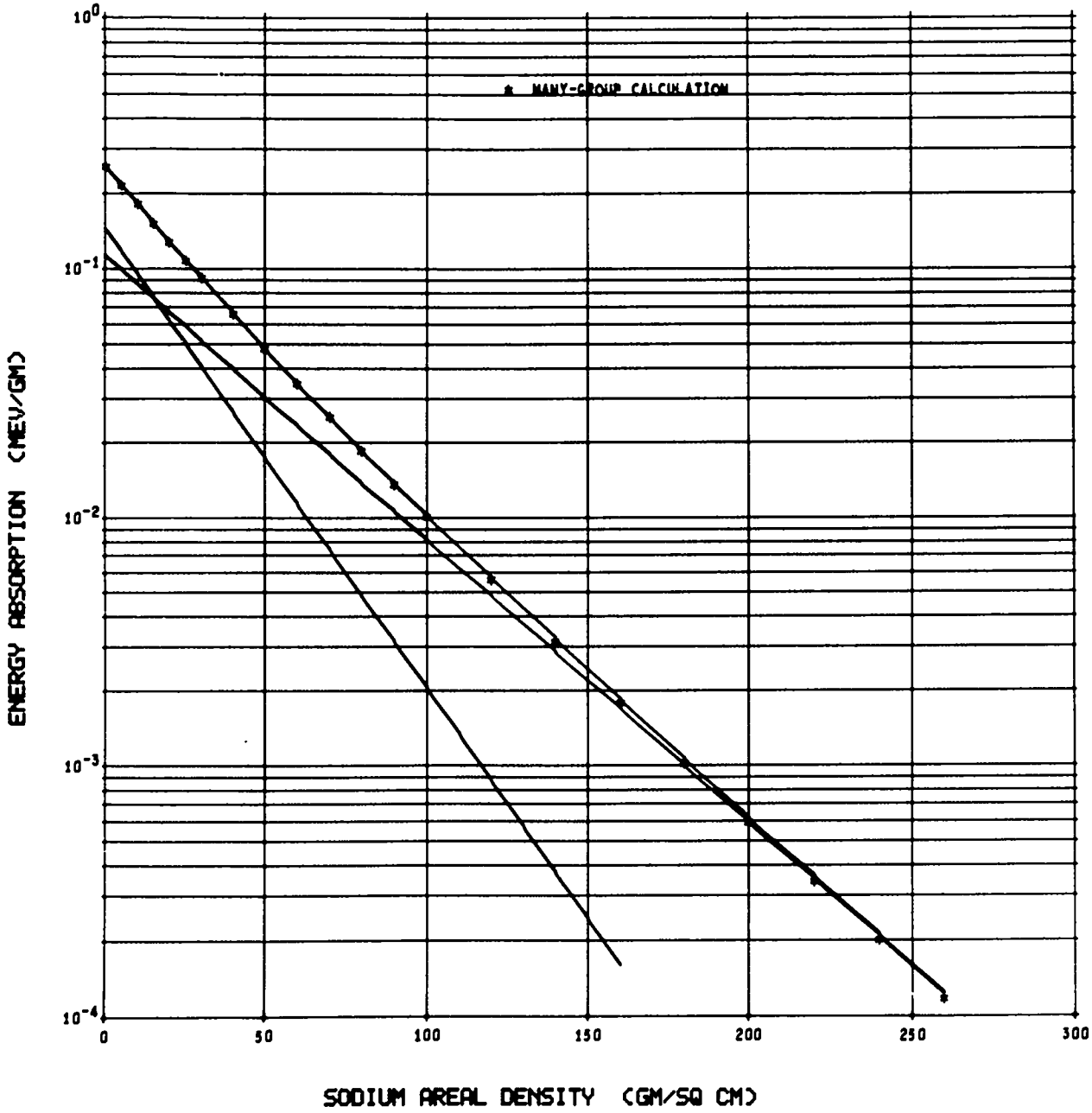
SODIUM SPECTRUM * TWO EXPONENTIAL FIT OF ABSORBED DOSE IN TISSUE
* MANY-GROUP CALCULATION
ENERGY ABSORPTION (MEV/GM)
SODIUM AREAL DENSITY (GM/SQ CM)
10^0
10^-1
10^-2
10^-3
10^-4
0
50
100
150
200
250
300

Fig. 17

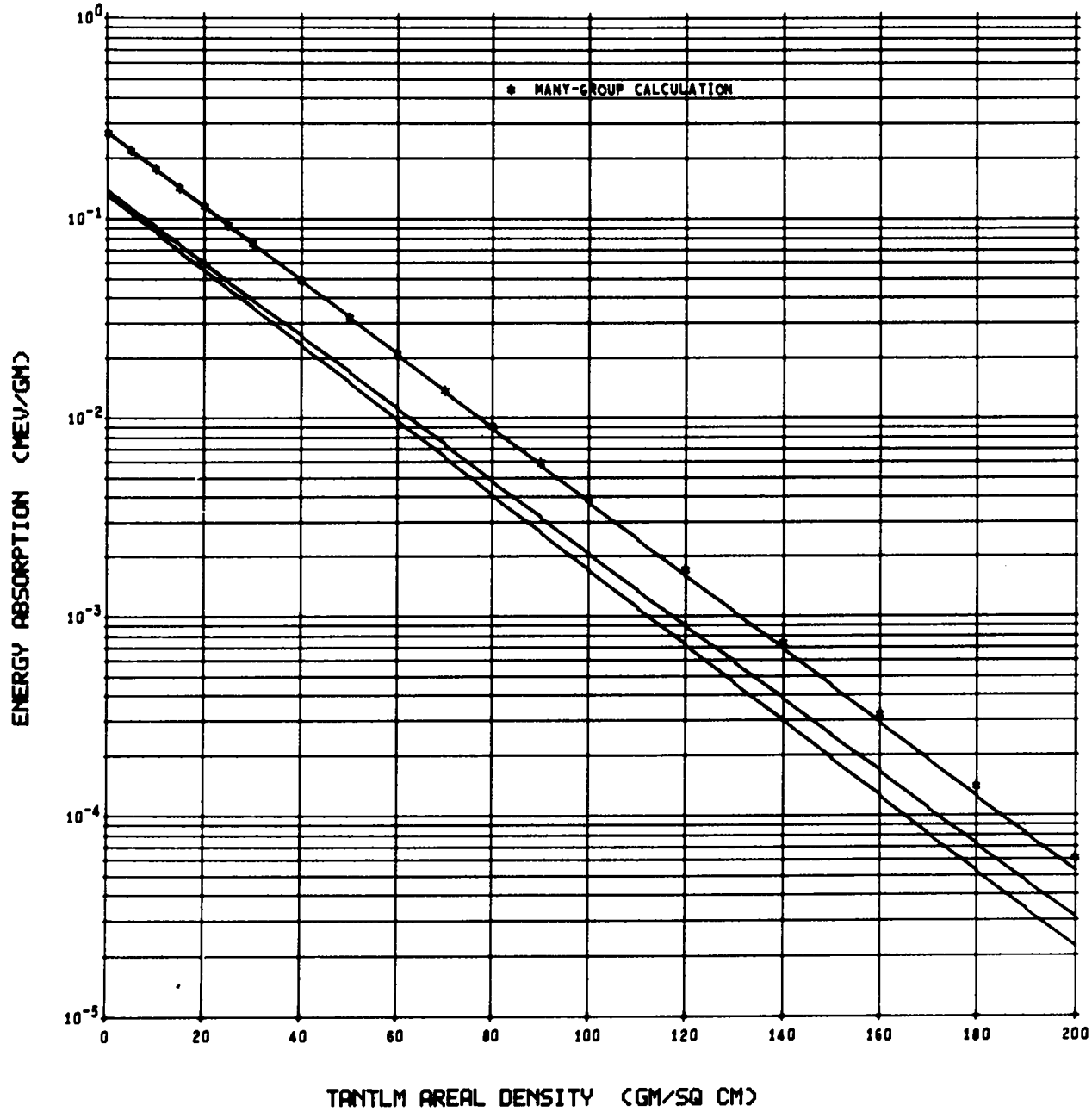
SODIUM SPECTRUM * TWO EXPONENTIAL FIT OF ABSORBED DOSE IN IRON
* MANY-GROUP CALCULATION
ENERGY ABSORPTION (MEV/GM)
TANTLM AREAL DENSITY (GM/SQ CM)
10^0
10^-1
10^-2
10^-3
10^-4
10^-5
0
20
40
60
80
100
120
140
160
180
200

Fig. 18

Fig. 19

SODIUM SPECTRUM * TWO EXPONENTIAL FIT OF ABSORBED DOSE IN TANTLM

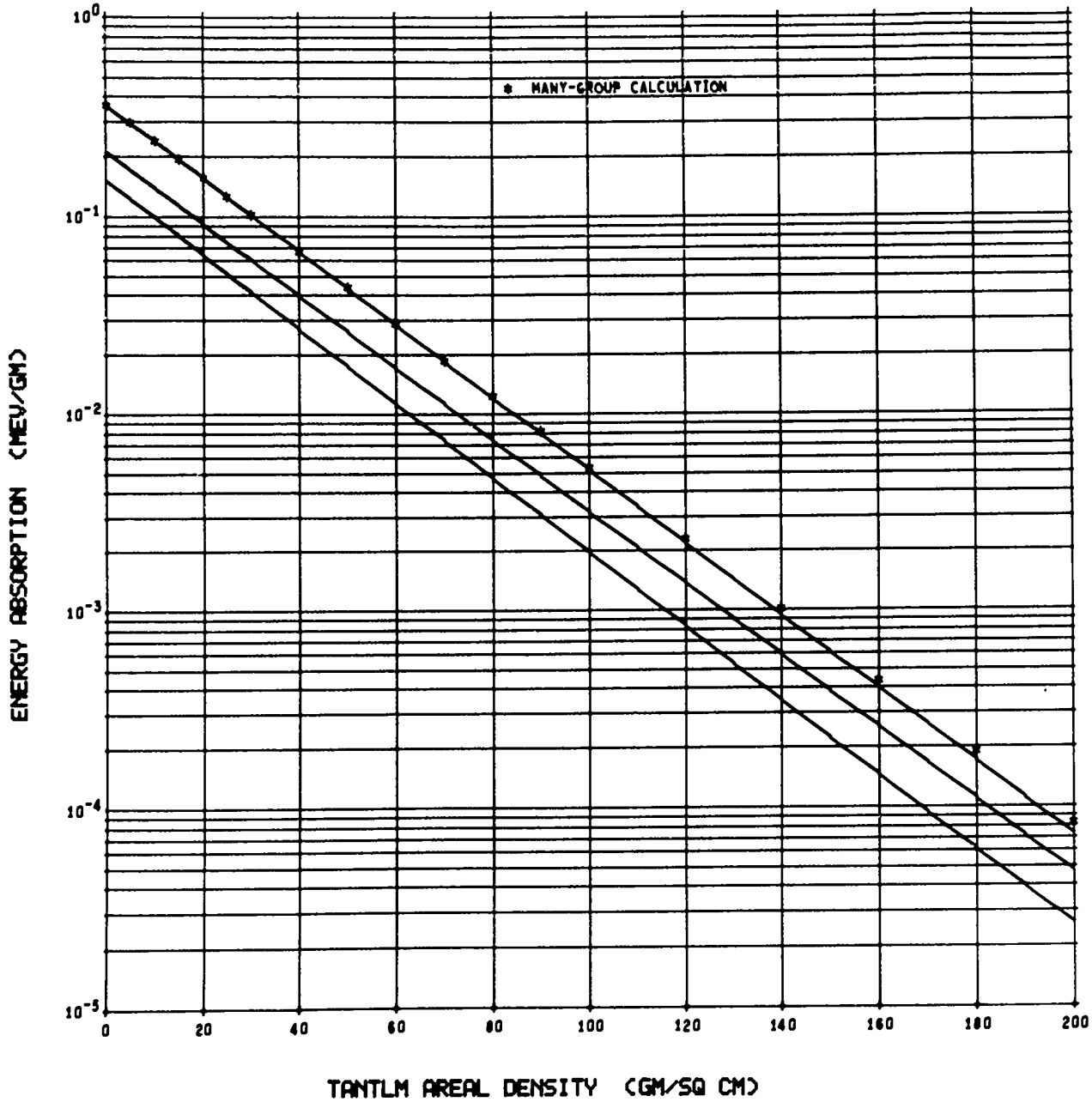

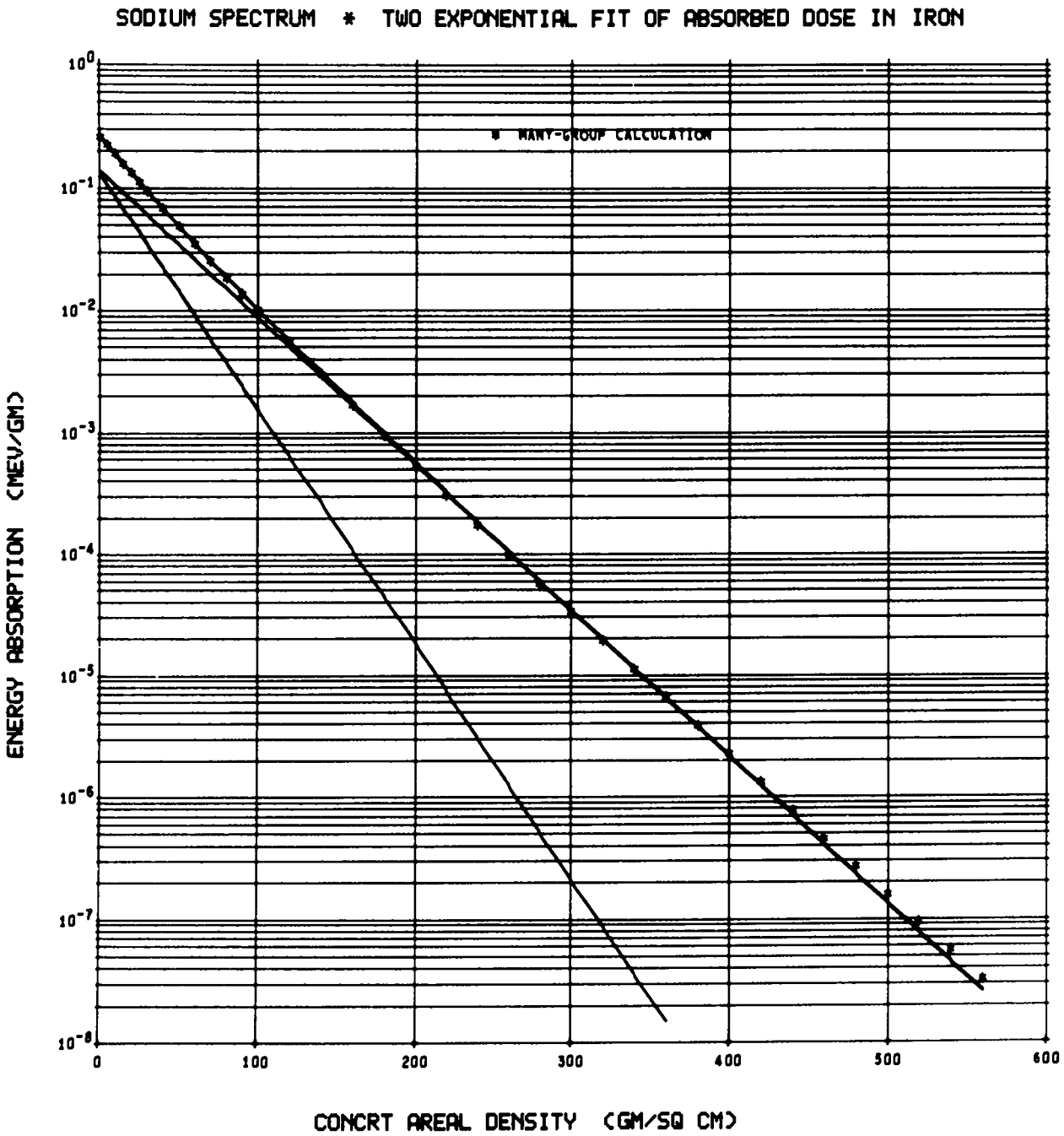
SODIUM SPECTRUM * TWO EXPONENTIAL FIT OF ABSORBED DOSE IN IRON
* MANY-GROUP CALCULATION
ENERGY ABSORPTION (MEV/GM)
CONCRT AREAL DENSITY (GM/SQ CM)
10^0
10^-1
10^-2
10^-3
10^-4
10^-5
10^-6
10^-7
10^-8
0
100
200
300
400
500
600

Fig. 20

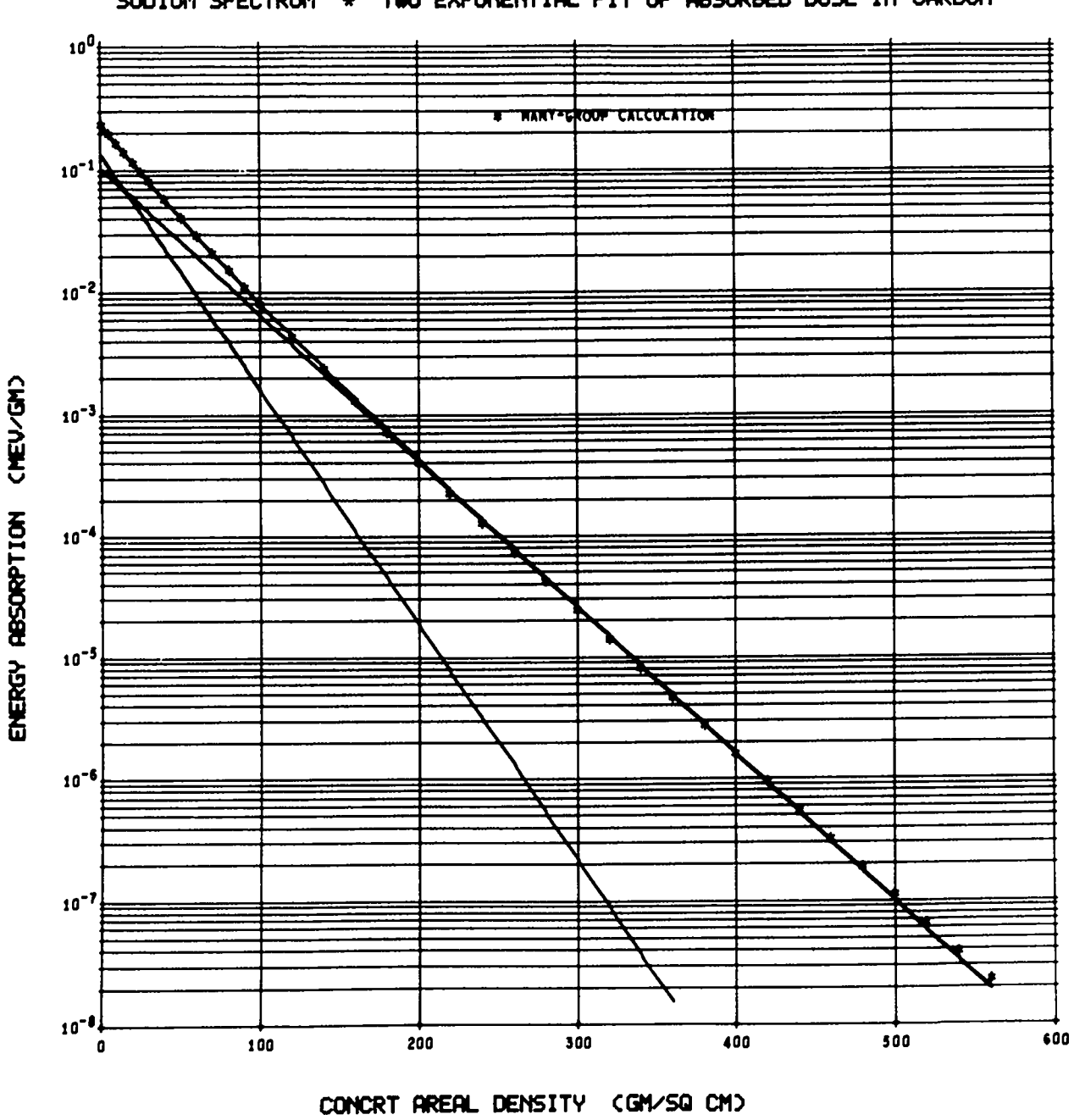
SODIUM SPECTRUM * TWO EXPONENTIAL FIT OF ABSORBED DOSE IN CARBON
* MANY-GROUP CALCULATION
ENERGY ABSORPTION (MEV/GM)
CONCRT AREAL DENSITY (GM/SQ CM)
10^0
10^-1
10^-2
10^-3
10^-4
10^-5
10^-6
10^-7
10^-8
0
100
200
300
400
500
600

Fig. 21

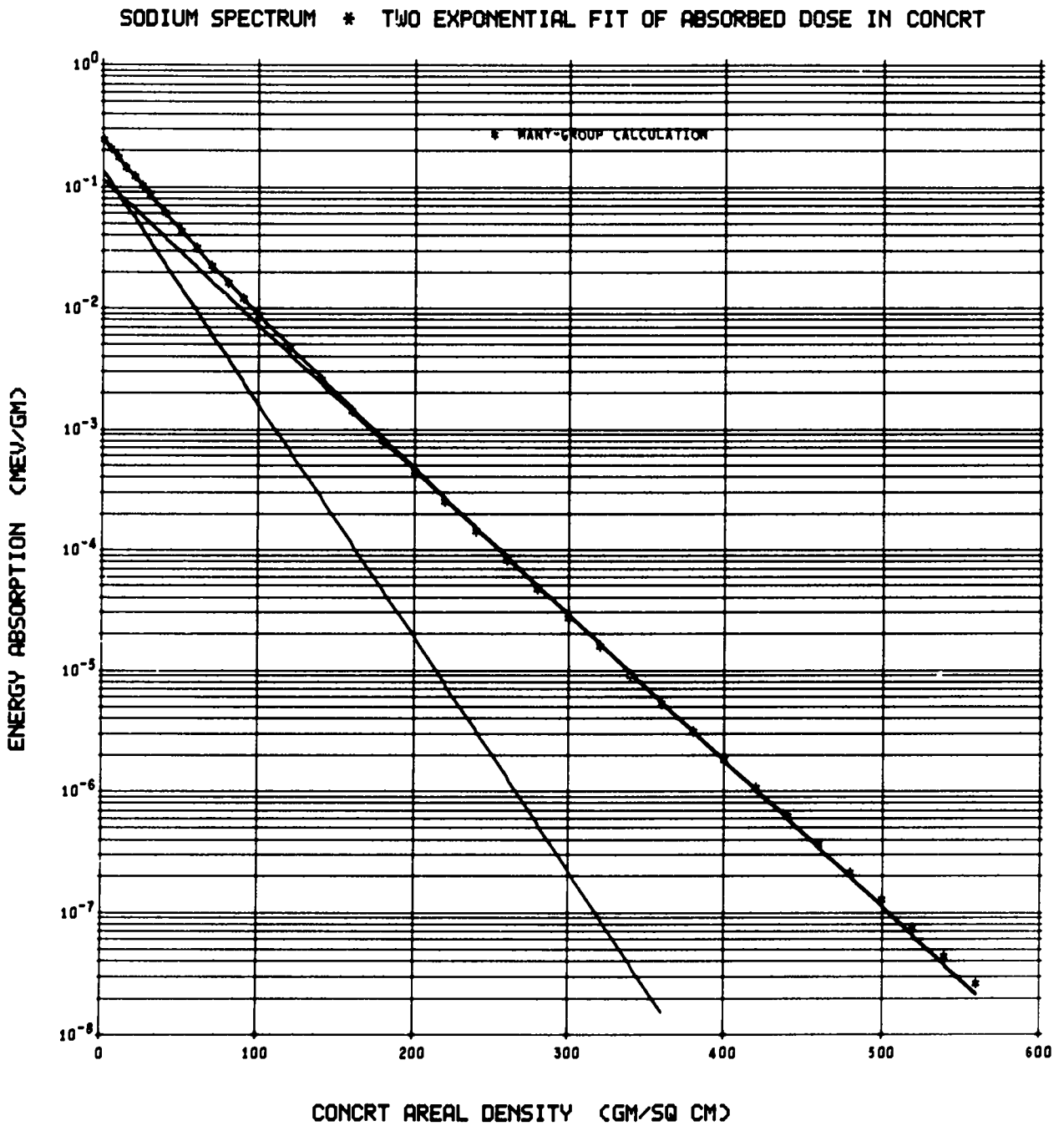
SODIUM SPECTRUM * TWO EXPONENTIAL FIT OF ABSORBED DOSE IN CONCRT
* MANY-GROUP CALCULATION
ENERGY ABSORPTION (MEV/GM)
10^{0}
10^{-1}
10^{-2}
10^{-3}
10^{-4}
10^{-5}
10^{-6}
10^{-7}
10^{-8}
0
100
200
300
400
500
600
CONCRT AREAL DENSITY (GM/SQ CM)

Fig. 22

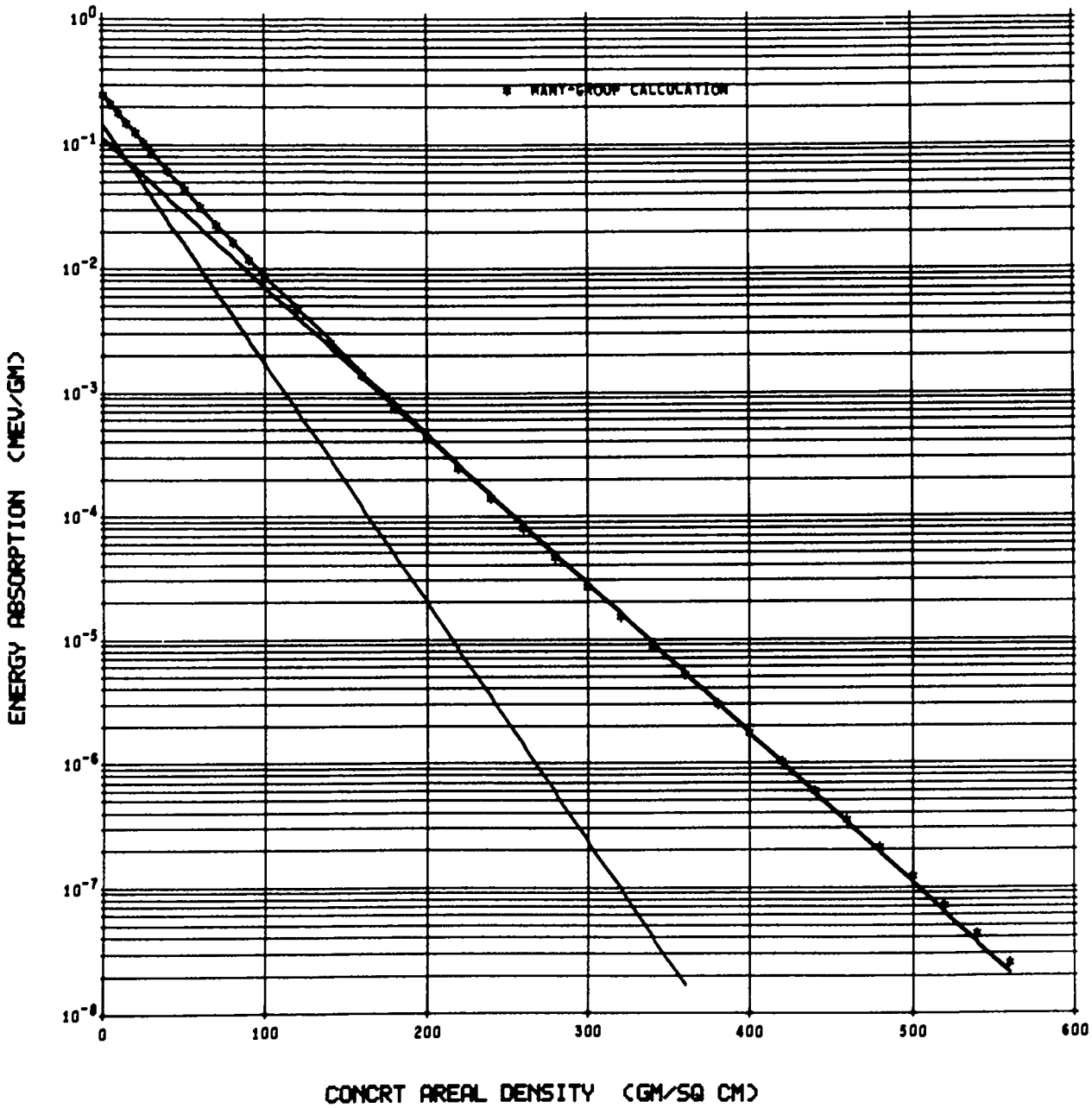
SODIUM SPECTRUM * TWO EXPONENTIAL FIT OF ABSORBED DOSE IN TISSUE
* MANY-GROUP CALCULATION
ENERGY ABSORPTION (MEV/GM)
10^{0}
10^{-1}
10^{-2}
10^{-3}
10^{-4}
10^{-5}
10^{-6}
10^{-7}
10^{-8}
0
100
200
300
400
500
600
CONCRT AREAL DENSITY (GM/SQ CM)

Fig. 23